ASPECTS OF THE DE HAAS-VAN ALPHEN EFFECT IN THE DILUTED ALLOY GOLD-CHROMIUM

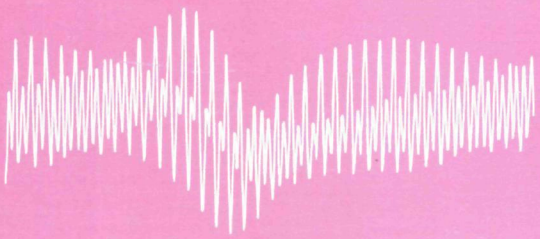

Paul Reinders

ASPECTS OF THE DE HAAS - VAN ALPHEN EFFECT IN THE DILUTED ALLOY GOLD-CHROMIUM

ASPECTS OF THE DE HAAS - VAN ALPHEN EFFECT IN THE DILUTED ALLOY GOLD-CHROMIUM

PROEFSCHRIFT

TER VERKRIJGING VAN DE GRAAD VAN DOCTOR IN DE
WISKUNDE EN NATUURWETENSCHAPPEN
AAN DE KATHOLIEKE UNIVERSITEIT TE NIJMEGEN, OP GEZAG VAN
DE RECTOR MAGNIFICUS PROF.DR. J.H.G.I. GIESBERS
VOLGENS BESLUIT VAN HET COLLEGE VAN DEKANEN
IN HET OPENBAAR TE VERDEDIGEN
OP MAANDAG 12 DECEMBER 1983
DES NAMIDDAGS TE 2.00 UUR PRECIES

door

PAULUS HENDRIKUS PETER REINDERS

geboren te Helden-Panningen

druk: drukkerij trio-print nijmegen bv

PROMOTOR: PROF.DR. A.R. DE VROOMEN

Bij deze wil ik iedereen bedanken die aan dit proefschrift hebben meegeholpen.
In het bijzonder wil ik vermelden:

Bennie Stortelder voor de technische ondersteuning en de vele discussies,

Louis Schreurs en Hein Weijers voor het groeien van de kristallen,

Lore Dekkers voor het verzorgen van het manuscript,

Doug Lowndes voor zijn enthousiasme en de stimulans bij het opzetten van het onderzoek,

Mart Ament voor zijn niet-lineaire kleinste kwadraten programma,

de medewerkers van de afdeling, die zorgdraagt voor de vloeibare gassen,

de afdeling illustratie en fotografie

het Hoge Magneten Laboratorium Nijmegen,

de instrumentmakerij en de afdeling electronica van de faculteit der Wiskunde en Natuurwetenschappen van de K. Universiteit te Nijmegen.

Contents

In 1930 W.J. de Haas and P.W. van Alphen reported an oscillatory behaviour of the diamagnetic susceptibility (the dHvA-effect) of bismuth single-crystals at 20.4 K and 14.2 K versus magnetic field, measured with the Faraday method requiring an inhomogeneous magnetic field across the crystal. L. Landau, also that year, published his famous article on diamagnetism of metals, quoted by de Haas and van Alphen. Landau wrote: "...$\mu H \ll kT$. This condition is no longer fulfilled at very low temperatures and in strong fields. On account of this, the latter case should lead to a complicated, no longer linear dependence of the magnetic moment on H, which should have a very strong periodicity in the field. Because of this periodicity, it should be hardly possible to observe this phenomenon experimentally, since on account of the inhomogeneity of the existing field, an averaging will occur.". However, the link between this sentence and the measurements wasn't made.

R. Peierls' theory (1933), an extension of Landau's theory for a cubic lattice, agreed qualitatively with the general features of the effect and M. Blackman (1938) could fit the experimental curves with the theoretical ones.

D. Shoenberg reported in 1939 results on bismuth measured with the torque method, carried out in the Institute for Physical Problems of the Academy of Sciences of the U.S.S.R. For political reasons (Hoch, 1983) he published in the appendix of his paper a new derivation of the dHvA effect by Landau.

Landau obtained an explicit formula for the susceptibility for ellipsoidal Fermi surfaces as a function of field contrary to Blackman who had to deduce the susceptibility by graphical computation, because the susceptibility and the field were given in implicit form by him, but no new physical assumption was required in this new derivation, it was only a matter of mathematics. It was

the first time that the susceptibility was written as a product of a temperature damping factor and a sine factor (see eq. 1, chapter II).

Onsager (1952) was the first who showed that the period of the dHvA oscillations was inversely proportional to the extremal area of the cross-section of the Fermi surface, but he wasn't understood, because he was talking in geometrical terms and in Cambridge, with Russia the center of the dHvA-effect at that time, one preferred only algebraic quantities and integrals (Pippard in Hoch, 1983). The complete mathematical solution of the dHvA-effect was given by I.M. Lifshitz and A.M. Kosevich (1955).

In a magnetic field $\underline{H}$ an electron in the wave packet approximation, moves on a helical path of constant energy, the classical cyclotron orbit, with cyclotron frequency $\omega_c = eH/m_c$. The area enclosed by the projection of the cyclotron orbit on a plane perpendicular to $\underline{H} = \text{curl } \underline{A}$ has to be quantized according to

$$\int \underline{p} \cdot d\underline{r} = \int (\hbar\underline{k} - e\underline{A}) \cdot d\underline{r} = (n + \gamma)\, h$$

(Bohr-Sommerfeld quantization) given by Onsager with $\gamma = 1/2$ for the free electron model (the value of γ should be very close to 1/2 for other models and experiment gives values approximately 1/2 (Gold, 1968; Coleridge, Templeton, 1972)).

This relation is identical with magnetic flux quantization or angular momentum quantization in the direction of $\underline{H}$. In $\underline{k}$-space the allowed states by the magnetic field are redistributed on Landau tubes (fig. I-1). The quantization in the direction of the magnetic field is not altered. The cross-sections of these tubes normal to H are quantized according to the above equation, and so the allowed areas A_n in k-space are

$$A_n = 2\pi\ (n + \gamma)\ eH/\hbar.$$

If H increases, the cylinders, for a free electron model, expand and the n-th tube is approaching the extremal cross-section of the Fermi-surface (fig. I-1). This corresponds to an increase of the free energy to a maximum. After the complete depletion of the states of this tube if H increases further, the electrons are redistributed, mostly on lower energy states, thus producing a lowering of the free energy. With further increase of the field the Landau cylinders expand, the free energy increases again and reaches a new maximum, when the (n-1)th cylinder approaches the extremal cross-section etc. The maxima of this oscillation occur when

$$A_n = 2\pi\ (n + \gamma)\ eH/\hbar = A_{ext} \quad \text{or} \quad n + \gamma = F/H \quad \text{with}$$

$$F = A_{ext}\ \hbar/(2\pi e),$$

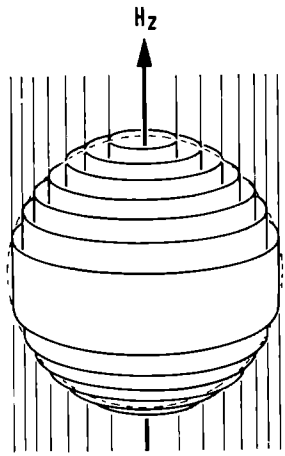

Fig. I-1 The effect of a magnetic field H parallel with $\hat{z}$ on the regions of k-space which can be occupied by electrons. The states constitute a series of infinite cylinders, all coaxial and parallel to H. The limit of occupancy set by the Fermi energy resembles the field-free Fermi sphere in coarse detail (Chambers, 1956).

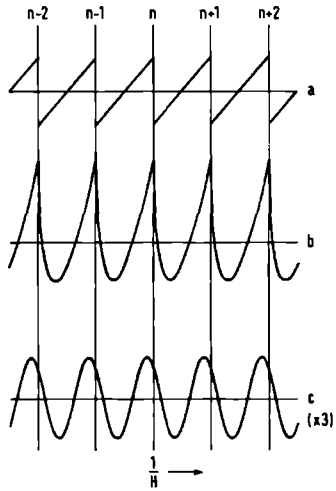

Fig. I-2

(a) The saw-tooth variation of the oscillatory part of the magnetization for a thin slice through the Fermi surface at absolute zero. The numbers n, n±1, ... indicate the quantum number of the highest occupied Landau level at the instant of depletion.
(b) The oscillatory magnetization at absolute zero obtained by summing the saw-tooth contributions from thin slices in the neighbourhood of an extremal area of cross section; if (a) refers to such an extremal section, then the cusps in (b) correspond to the discontinuities in (a), but the vertical scales for (a) and (b) are arbitrary.
(c) Magnetization oscillations as in (b), but at a finite temperature which corresponds to setting $T = 1^{o}K$ if $\mu = 1$ and $H = 5$ T. The vertical scale has been magnified three times with respect to that in (b) (Gold, 1968).

A_{ext} the area of the extremal cross-section. Thus the frequency of this oscillation of the free energy, which gives also an oscillation of the magnetization, the dHvA effect, is F in the 1/H domain (see also fig. I-2). It is obvious that only the electrons in the extremal cross-section of the Fermi surface contribute to the dHvA effect (fig. I-1). The temperature affects the sharpness of the Fermi surface, and the scattering of the electrons affects the sharpness of the Landau-levels, which both decrease the amplitude of the signal. For high temperatures these influences are identical. In 1952 R.B. Dingle proposed an exponential damping factor in the susceptibility due to finite lifetimes of the electrons, which corresponds with a Lorenztion broadening of the energy levels. He also introduced the effect of spin of the electrons on the amplitude.

In the mean time the experimental work made a big step. Shoenberg (1952) developed the pulsed field system. This system dominated until late into the sixties. During the experiments involving the use of high magnetic fields to study dHvA in the noble metals, Shoenberg (1962) noticed that the harmonic content of the observed signals was much stronger than is predicted by the Lifshitz-Kosevich theory (eq. II-1). He proposed that the reason for this is that the effective magnetizing field which conduction electrons see is not $\underline{H}$ but instead is the total magnetic induction

$$\underline{B} = \underline{H} + 4\pi(1 - N_e)\underline{M}$$

where $\underline{M}$ is the (oscillatory) dHvA magnetization of the sample itself, and N_e is the sample's demagnetization factor ($0 \leq N_e \leq 1$). Thus, the conduction electrons magnetically interact (MI) with themselves, by responding to a $\underline{B}$ field which includes their own oscillatory magnetization. Shoenberg's conjecture has since been confirmed on thermodynamic and experimental grounds by Pippard

(1963), by Condon (1966) and by Shoenberg and Vuillemin (1966).

The low frequency (no skindepth problems) magnetic field modulation technique (Goldstein et al., 1965; Stark and Windmiller, 1968; Windmiller and Ketterson, 1968), described in chapter III.1, gave a complete revolution. This technique is based on a method proposed by D. Shoenberg and P.J. Stiles (1963) who used a modulation frequency in the skindepth region (the mega-cycle region). Now it was possible to check in detail the dHvA-formula (chapter I.1). The dHvA effect was not anylonger only a tool for measuring the Fermi-surface alone but effective masses of the conduction electrons, impurity scattering, electron-phonon interaction, exchange interaction, pressure dependent Fermi-surfaces, g-factors, etc. could also be studied.

The review articles available are: Lifshitz, Kaganov (1963); Gold (1968); Springford (1971,1980); Chung et al. (1978) and Lengeler (1978).

II. Theory

II.1 The de Haas - van Alphen effect

The rigorous quantitative theory of the dHvA-effect was provided principally by Lifshitz and Kosevich (1955). Their (LK) result for the magnetization, magnetic moment per unit volume, is

$$\underline{M} = -\hat{m}/2 \sum_{r=1}^{\infty} \sum_{\sigma} C_r D^r \sin[2\pi r(F/H - \gamma) + p\pi/4 - \sigma\pi rS] \qquad (1)$$

with r the dHvA harmonic index, σ + (-) for spin up (down) electrons, and

$$C_r = \frac{\nu TF}{\sqrt{\xi r H}\ 2\sinh(r\lambda\mu T/H)} \qquad (2)$$

$$D^r = e^{-\lambda r \mu X/H} \qquad (3)$$

$$S = (\mu/2)\, g_c \qquad (4)$$

$$\nu = (4k_B/\sqrt{2\pi})(e/\hbar)^{3/2} = 1.304\ (T^{1/2}/K) \qquad (5)$$

$$\lambda = 2\pi^2\, k_B\, m_o/(e\hbar) = 14.69\ (T/K) \qquad (6)$$

where F ($\equiv F(\theta,\phi)$) is the dHvA frequency ($=\hbar A_{ext}/(2\pi e)$) in 1/H for the field direction H, specified by the spherical coordinates (θ,ϕ), A_{ext} is the extremal cross-section area of the Fermi surface normal to the magnetic field, γ is the Onsager phase factor (= 1/2 for free electrons), p=-1 (+1) if the extremal Fermi surface cross-section is a maximum (minimum) with respect to the variation of k_H, ξ is the Fermi surface curvature factor $|\partial^2 A_{ext}/\partial k_H^2|$, μ is the cyclotron effective mass m_c in units of

the free electron mass m_o, k_B is Boltzmann's constant,

$$\hat{m} = \hat{H} - \frac{1}{F}\frac{\partial F}{\partial \theta}\hat{\theta} - \frac{1}{F\sin(\theta)}\frac{\partial F}{\partial \phi}\hat{\phi} \qquad (7)$$

g_c is the electronic cyclotron orbitally-averaged g-factor.

X, called the Dingle temperature, is the cyclotron orbital average of the electronic scattering rate τ_k^{-1}, at the point k on the Fermi surface,

$$X = \hbar/(2\pi k_B) \langle 1/\tau_k \rangle = \langle \Gamma \rangle /(\pi k_B) \qquad (8)$$

where $\langle \Gamma \rangle$ is the broadening (assumed to be Lorentzian) of the Landau levels (Brailsford, 1966).

Equations (1 to 8) demonstrate that a number of different parameters describing the properties of electrons in metals, can influence the amplitude and the phase of the dHvA oscillations.

Since only those electrons lying on narrow orbits, at the extremal cross-section of the Fermi surface, produce observable oscillations, then equation (1), in principle, provides a way of comparing experimental and theoretical values for a variety of electronic properties, for electrons in well-defined states on the Fermi surface. This is an important advantage of dHvA measurements, in comparison with bulk transport coefficient measurements, which provide only a weighted average of electronic properties over the entire Fermi surface.

From an experimental point of view, the greatest significance of the LK expression for M is that it is a harmonic series: each term in the series depends in a complicated way on a wealth of electronic parameters. It is not possible to determine all of these parameters from measurements of the amplitude and phase of a single harmonic alone.

An additional complication is the Landau level broadening (primarily due to electron scattering by impurity atoms and by crystalline defects), and the thermal broadening of the Fermi surface, all contribute to an approximately exponential attenuation of the higher harmonics.

For more details see for example Ziman (1964), Gold (1968) and Springford (1971, 1980).

II.2 Magnetic impurities

Some transition metal elements produce local magnetic moments when they are dissolved in noble metal (Cu, Ag, Au). The local moment $\underline{S}$ is associated with the d-states of the impurity. The local magnetic moment can interact with the conduction electron moment $\underline{s}$ via an effective exchange interaction, for simplicity, an isotropic Heisenberg exchange Hamiltonian,

$$H_{ex} = -c\, J\, \underline{S}\cdot\underline{s} \qquad (9)$$

with exchange constant J (<0) >0 for (anti)ferromagnetic exchange, and local moment concentration c.

Together with the Zeeman Hamiltonian

$$H_Z = -\underline{\mu}\cdot\underline{H} = +g\mu_B\, \underline{s}\cdot\underline{H} \qquad (10)$$

we get an energy shift for a spin up electron (fig. II.1)

$$\Delta E/2 = \langle H_{ex} + H_Z \rangle = -cJ/2 \langle S_z \rangle + (g\mu_B/2)H \qquad (11)$$

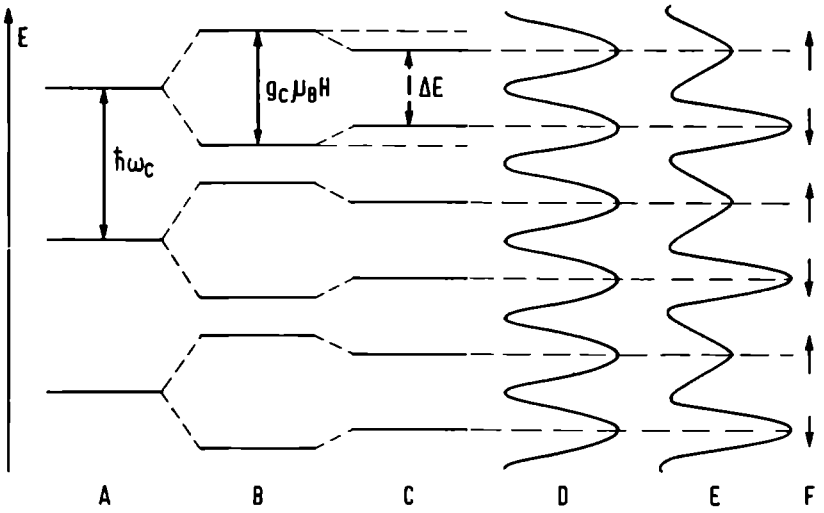

Fig. II-1 Density of states

A. A magnetic field causes a quantization of the energy levels, separated by $\hbar\omega_C$.

B. The spin of the electrons results in a splitting of each energy level of $g_C\mu_B H$.

C. An exchange interaction produced by magnetic impurities gives a new spin splitting ΔE (eq. II-11) (shown is an anti-ferromagnetic exchange).

D. The levels are broadened by scattering.

E. The magnetic impurities give a spin dependent lifetime, so that the broadening of spin up and spin down electron levels are different.

F. The direction of the spin:

+ parallel magnetic field (spin up),

+ anti-parallel magnetic field (spin down).

where $< S_z >$ is a function of T and H. The component of $\underline{S}$ along $\underline{H}$ reflects the polarization of the local moment by the applied field. Thus we can define an effective g-factor

$$g_c' = g_c + H_{ex}/H \tag{12}$$

with $$H_{ex} = -c\, J < S_z > /\mu_B. \tag{13}$$

There is a reason to expect the scattering rates for spin up and spin down electrons to be unequal, corresponding to the unequal Landau level broadening shown in fig. II-1.

Thus

$$\underline{M} = -(\hat{m}/2)\sum_{r=1}^{\infty}\sum_{\sigma} C_r D^r E^{\sigma r} \sin[2\pi r(F/H - \gamma) + p\pi/4 - \sigma\pi r S'] \tag{14}$$

with

$$S' = (\mu/2)g_c' = \mu/2(g_c + H_{ex}/H) \tag{15}$$

$$D = \exp(-\lambda\mu X/H) \tag{16}$$

$$E = \exp(-\lambda\mu\delta X/H) \tag{17}$$

and X is the mean Dingle temperature

$$X = (X^+ + X^-)/2 \tag{18a}$$

and $$\delta X = (X^+ - X^-)/2 \tag{18b}$$

It is more useful to write this formula as:

$$\underline{M} = -\hat{m} \sum_{r=1}^{\infty} A_r' C_r D^r \sin[2\pi r(F/H-\gamma)+p\pi/4+\Delta\theta_r+(1-q_r')\pi/2] \quad (19)$$

with $A_r' = [E^{2r}+E^{-2r}+2\cos(2\pi rS')]^{1/2}/2$ (20)

$$\Delta\theta_r = \tan^{-1}[\tan(\pi rS')\tanh(r\lambda\mu\delta X/H)] \quad (21)$$

$q_r' = +1$ for $\cos(\pi rS') > 0$

$= -1$ for $\cos(\pi rS') < 0$.

q_r' and S' are here introduced to distinguish them from the unprimed quantities which have been reserved only for no spin dependent scattering and no exchange.

It is conventional to express the dHvA effect in terms of interaction self-energies, because then many body effects, for instance electron-phonon interaction, can be introduced easier.

The theory of the dHvA effect in the Green's function formalism developed by Fowler and Prange (1965) and Engelsberg and Simpson (1970) gives for the magnetization

$$\underline{M} = -\nu TF/(\sqrt{\xi}H)\hat{m}/2 \sum_{r=1}^{\infty} \sum_{\sigma} 1/r^{1/2} \sum_{n=0}^{\infty} \exp\{-2\pi r(\omega_n-\Sigma''_{n\sigma})\, m_c/(e\hbar H)\}$$

$$\sin\{2\pi r(F/H - (\Sigma'_{n+} + \Sigma'_{n-})m_c/(2e\hbar H) - \gamma)$$

$$+ p\pi/4 - \sigma\pi r(S + (\Sigma'_{n+} - \Sigma'_{n-})m_c/(e\hbar H))\} \quad (22)$$

in the case of magnetic impurities and high quantum numbers (Shiba, 1973), with $\omega_n = (2n+1)\pi K_B T$.

$\Sigma'_{n\sigma}$ and $\Sigma''_{n\sigma}$ are the real and imaginary part of the self-energy $\Sigma_\sigma(i\omega_n) = \Sigma'_{n\sigma} - i\,\Sigma''_{n\sigma}$ which is an orbital average.

It is possible to make the following correspondences:

- a frequency shift $\Delta F = -(\Sigma'_+ + \Sigma'_-)m_c/(2e\hbar)$ (23)
- a g shift $\Delta g = (\Sigma'_+ - \Sigma'_-)/\mu_B H)$ (24)
- a Dingle temperature for the spin up and spin down electrons $X^+ = (-\Sigma''_+)/(2\pi k_B)$ and $X^- = (-\Sigma''_-)/(2\pi k_B)$ with $\Sigma(0) = \Sigma'_+ - i\,\Sigma''_-$.

This is only true for $k_B T >> (e\hbar/m_c)H = \hbar\omega_c$ or if it happens that $\Sigma(i\omega_n)$ can be replaced by $\Sigma(0)$ (Fenton, 1976).

According to Fenton (1976)

$$\Sigma'_0 = -1/2\ c_0 J \langle S_z \rangle + cV \qquad (25).$$

The first term describes the "Kondo" effects (J is the bare exchange interaction of the Kondo hamiltonian (Kondo, 1964; Heeger, 1969), $\langle S_z \rangle$ is the expectation value for a single impurity, including all Kondo effects), the second the potential scattering.

From this one can see that the dHvA is a direct probe of both J and $\langle S_z \rangle$ in the Kondo effect.

Putting Fenton's results into Shiba's equation for ΔF and Δg we get:

$$\Delta F/H = -cV/(\hbar\omega_c) \quad \text{(pure potential effect)} \qquad (26)$$

$$\Delta g = -cJ \langle S_z \rangle /(\mu_B H) \quad \text{(pure magnetic effect)} \qquad (27).$$

The other formulae do not give such clean results (a mixing up of magnetic and potential scattering).

Substituting

$$\underline{B} = \underline{H} + 4\pi\,(1 - N_e)\,\underline{M} \tag{28}$$

for $\underline{H}$ only in the sine factor because also replacing $\underline{H}$ by $\underline{B}$ in the amplitude factors C_r, D_r and E^r has a negligible effect ($|4\pi\underline{M}| \ll H$), we get an implicit function for $\underline{M}$:

$$\underline{M} = \hat{m} \sum_{r=1}^{\infty} M_r \sin\left[2\pi r\left(\frac{F}{H+4\pi(1-N_e)M} - \gamma\right) + \theta_r\right] \tag{29}.$$

We have taken $\underline{M}$ and $\underline{H}$ parallel.
For $|4\pi M/H| \ll 1$ we get

$$\underline{M} = -\hat{m} \sum_{r=1}^{\infty} A_r' C_r D^r \sin[r(x_o - k'M) + p(\pi/4) + \Delta\theta_r + (1-q_r')\pi/2] \tag{30}$$

with $$k' = (1-N_e)8\pi^2 F/H^2 \tag{31}$$

and $$x_o = 2\pi(F/H - \gamma) \tag{32}.$$

We define the "weak MI" limit by the condition

$$|k' A_1' C_1 D| < 1 \tag{33}$$

which corresponds physically to the requirement that the dHvA fundamental oscillations never become multi-valued as a function of the applied field H (see Pippard, 1963).

Adopting the iterative expansion technique of Phillips and Gold (1969), we get for the n^{th} approximation

$$\underline{M}^{(n)} = -\hat{m} \sum_{r=1}^{\infty} A_r' C_r D^r \sin[r(x_o - k' \underline{M}^{(n-r)}) + \Delta\theta_r + p(\pi/4) + (1-q_r')\pi/2] \tag{34}$$

with $\underline{M}^{(0)} = 0$. Carrying out this procedure we get for the third order approximation:

$$\begin{aligned}
\underline{M}^{(3)} = +\hat{m}[& A_1' C_1 D \sin(\theta_1^{LK}) \\
& + (k')^2 (A_1' C_1 D)^3/8 \sin(\theta_1^{MIp}) \\
& + (k'/2)(A_1' C_1 D)(A_2' C_2 D^2) \sin(\theta_1^{MIpq}) \\
& + A_2' C_2 D^2 \sin(\theta_2^{LK}) \\
& + (k'/2)(A_1' C_1 D)^2 \sin(\theta_2^{MI}) \\
& + A_3' C_3 D^3 \sin(\theta_3^{LK}) \\
& + (3/8)(A_1' C_1 D)^3 (k')^2 \sin(\theta_3^{MIq}) \\
& + (3k'/2)(A_1' C_1 D)(A_2' C_2 D^2) \sin(\theta_3^{MIpq})
\end{aligned} \tag{35}$$

with

$$\theta_1^{LK} = (x_o + p\pi/4 + \Delta\theta_1) - (1 + q_1')\pi/2$$

$$\theta_1^{MIp} = (x_o + p\pi/4 + \Delta\theta_1) + (1 - q_1')\pi/2$$

$$\theta_1^{MIpq} = (x_o + \Delta\theta_2 - \Delta\theta_1) + (q_1' - q_2')\pi/2$$

$$\theta_2^{LK} = (2x_o + p\pi/4 + \Delta\theta_2) - (1 + q_2')\pi/2$$

$$\theta_2^{MI} = (2x_o + 2p\pi/4 + 2\Delta\theta_1) - q_1'\pi$$

$$\theta_3^{LK} = (3x_o + p\pi/4 + \Delta\theta_3) - (1 + q_3')\pi/2$$

$$\theta_3^{MIq} = (3x_o + (p - 2q_1')3/4\pi + 3\theta_1 + \pi/2$$

$$\theta_3^{MIpq} = (3x_o + p\pi/2 + \Delta\theta_1 + \Delta\theta_2) - (q_1' + q_2')\pi/2 \qquad (36).$$

Perz en Shoenberg (1976) give the formula up to eight-order approximation. The amplitude coefficients of the various terms in equation (35) are in error by no more than 2% if

$$|k'A_1'C_1D| \leq .2$$

The effect of spin dependent scattering (SDS) and exchange interaction is to alter the resultant waveshape in both amplitude and phase from either of the usual LK or MI results. In particular, MI and SDS effects mix non-linearly. Thus, the MI and LK components at each harmonic no longer differ in phase by a simple, fixed amount (such as $p\pi/4$) as in pure metals.

If we define α_r as the phase angle by which the resultant r^{th} harmonic amplitude deviates from the pure LK component with SDS and exchange, we get

$$\theta_r = [rx_o + p\pi/4 - (1 + q_r')\pi/2] + \Delta\theta_r + \alpha_r \qquad (37),$$

$$T12 \equiv (2\theta_1 - \theta_2)^{OB} =$$

$$p\pi/4 + (1 + q_2')\pi/2 + (2\Delta\theta_1 - \Delta\theta_2) + 2\alpha_1 - \alpha_2 \qquad (38)$$

and $$T13 \equiv (3\theta_1 - \theta_3)^{OB} =$$

$$2p\pi/4 - (q_1' - q_3')\pi/2 + 3\Delta\theta_1 - \Delta\theta_3 + 3\alpha_1 - \alpha_3 \qquad (39).$$

Also by definition:

$$M3122 = [(M_3/M_1)/(M_2/M_1)^2]^{OB} \qquad (40)$$

$$M21 = (M_2/M_1)^{OB} \qquad (41)$$

and $$M31 = (M_3/M_1)^{OB} \qquad (42)$$

with M_i the amplitude of the i^{th} dHvA harmonic (in the appendix of Chung, Lowndes and Hendel (1978) the reader can find the α_i's and M_i's, which can be calculated by normal geometrical methods).

We have now five observables (with the upperscript "OB") which can be measured, and are independent on the gain of the electronic system. For the two phase differences (eq. 38 and 39) the very large phase x_o and the not accurately known Υ (Coleridge, Templeton, 1972) drops out. The first three observables depend on X through α_1 (a third order correction to the first harmonic caused by MI). This α_1 is such a small correction on the neck orbit for our samples, temperature and field range, that these three are independent on the mean Dingle temperature.

A computer-graphic technique provides the precise values (together with error estimates) for δX, X and S' if the observables

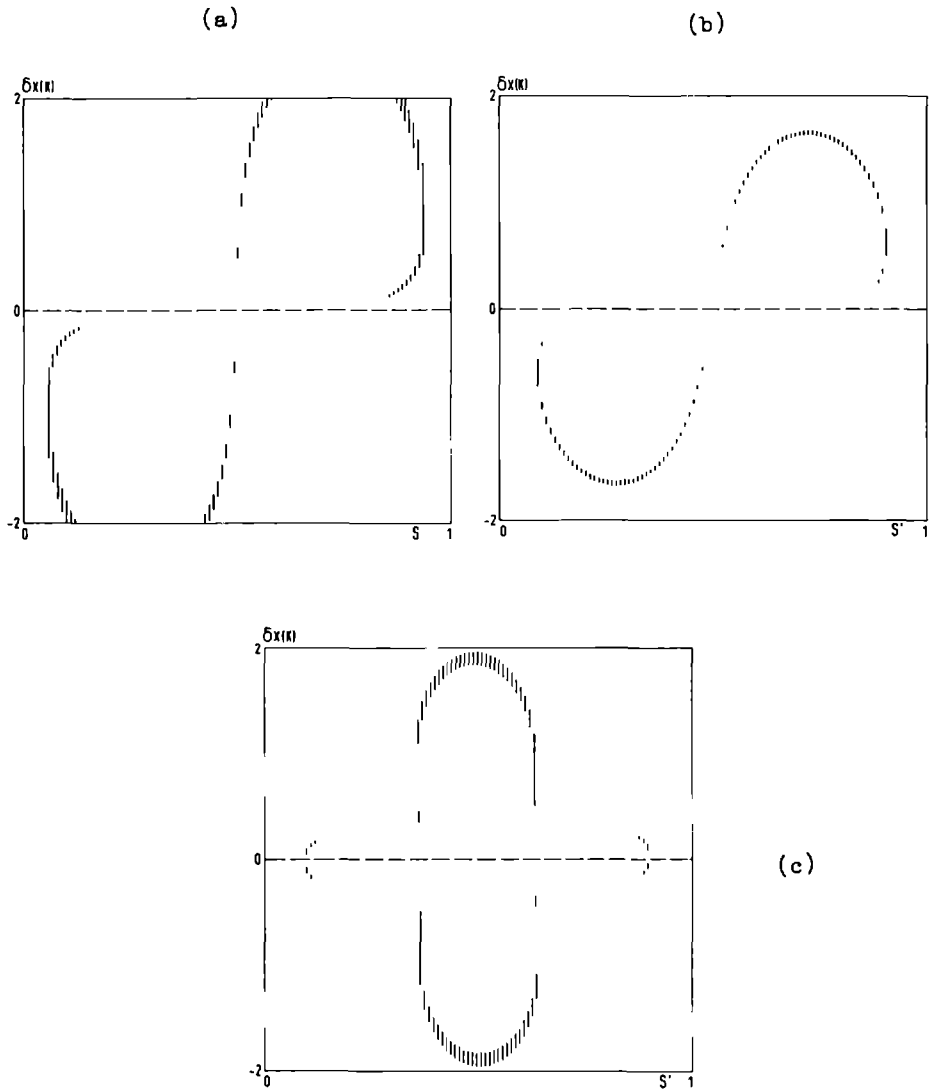

Fig. II-3 A solution for (δX, S′) using measured values of $2\theta_1-\theta_2$ (solid line), $3\theta_1-\theta_3$ (broken line) and M_3M_1/M_2^2 as described in the text for the <111> neck orbit (δX = .20 K , S′ = -.103).

are known. In the δX-S′ plane the computer searches for pairs of δX and S′, which produce the measured values of the three observables (eq. 37, 38, 39). Fig. II-2 illustrates the loci of the solutions (δX, S′). Combining these figures we get a point δX, S′ what corresponds to all the three measured values of the observables (fig. II-3). Because of the symmetries present, several sets of solutions are possible (δX, S′+n or -δX, -S′+n with n an integer).

Plotting the loci of the values of the observables which correspond to the errors in the measurements, we get the error for δX and S′ (fig. II-4). Fig. II-5 demonstrates the use of the observables M21 and M31 (eq. 41 and 42). This figure gives us X with an error estimate.

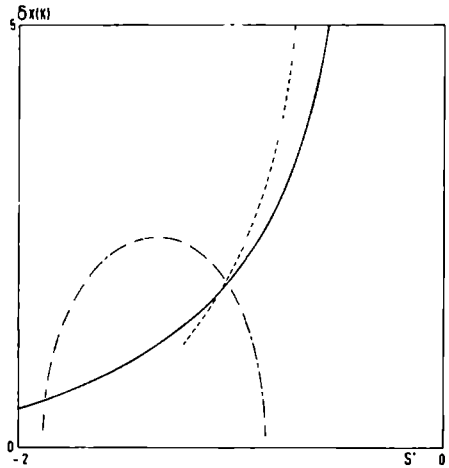

Fig. II-2 Plot of the loci of solutions (δX, S′) corresponding to measured values of $2\theta_1-\theta_2$ (a), $3\theta_1-\theta_3$ (b) and M_3M_1/M_2^2 (c). The slight assymetry is due to MI, while the broken plotted lines are due to discrete stepping of the computer search for solutions (Lowndes, Reinders).

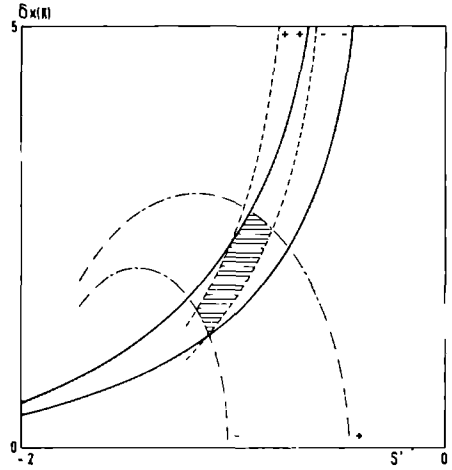

Fig. II-4 The error area (shaded) belonging to the unique solution (δX, S′) in fig. II-3 (+ : the measured observable minus its error; - : the value minus the error; δX = .20 ± .08 K; S′ = -.103 ± .015)

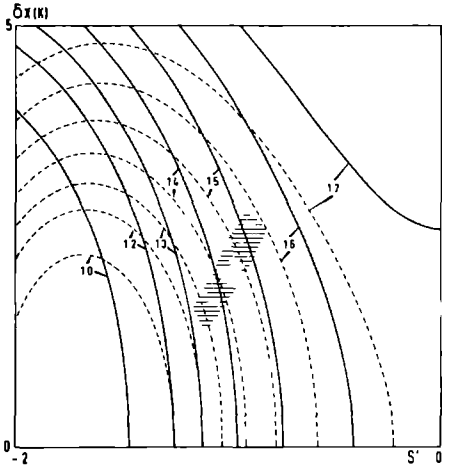

Fig. II-5 The loci of solutions of the observables M21 (solid lines) and M31 (broken lines) for the measured values with parameter X. The shaded area corresponds to the possible solutions of (δX, S′) (see fig. II-4) and gives with the parameter of the drawn lines the solution of X with the error (X = 1.44 ± .10 K).

To determine δX, X and S′ we need only three observables (e.g. T12, T13 and M21), but with five observables it is possible to reduce the errors and to remove the accidental π in the phases (section III.1). It is also possible that one or more observables can not be measured accurately enough. That is why we introduce the new observables

$$M211 = M2/(M1)^2 \tag{43}$$

$$M3111 = M3/(M1)^3 \tag{44}$$

and

$$T23 = 2\theta_3 - 3\theta_1 \tag{45}$$

The first two are nearly independent on X, but we have to know the gain of the electronic system (section III.1). At a magnetic field H and temperature T where it is possible to determine δX and S′ with the normal observables, we can calculate for instance M211 what gives us the desired gain factor (X is not needed). With this gain factor known we can increase the measuring range of our detection system (lower magnetic field, higher temperature and higher Dingle temperature) if the third harmonic has a no more measurable amplitude caused by scattering or temperature.

III. Experiment

III.1 Detection

The technique used is a further sophistication of the Shoenberg- Stiles method (Shoenberg and Stiles, 1963, 1964) called the large field amplitude modulation technique (Goldstein et al., 1965; Stark and Windmiller, 1968; Windmiller and Ketterson, 1968). It is particularly useful for waveshape measurements because of its "Bessel function spectrometer" action which makes it possible to enhance the amplitude of the higher dHvA harmonics at the expence of the fundamental (Alles and Higgins, 1974).

The sample is put in a magnetic field H, generated by a superconducting coil. A modulation field $h \cos \omega t$ is superimposed on the magnetic field:

$$H(t) = H + h \cos \omega t.$$

This gives a time-dependent magnetization of the sample. The detection of the magnetization is done with a compensating pick-up coil system (P.U.). This means the coil is made up of two identical coils which are wound counterwise and connected in series, so that the voltages induced by the modulation field are compensated. One of these coils contains the sample. The voltage V induced by the magnetization is:

$$V = G\, dM/dt$$

$$= G\, d/dt \left\{ \sum_{r=1}^{\infty} M_r \sin(2\pi r(F/H - Fh/H^2 \cos\omega t - \gamma) + \theta_r) \right\}$$

(we have approximated, as by MI (section II.3), $1/(H + h)$ by $1/H - h/H^2$ in the argument of the sines and neglected h in the amplitude factors).

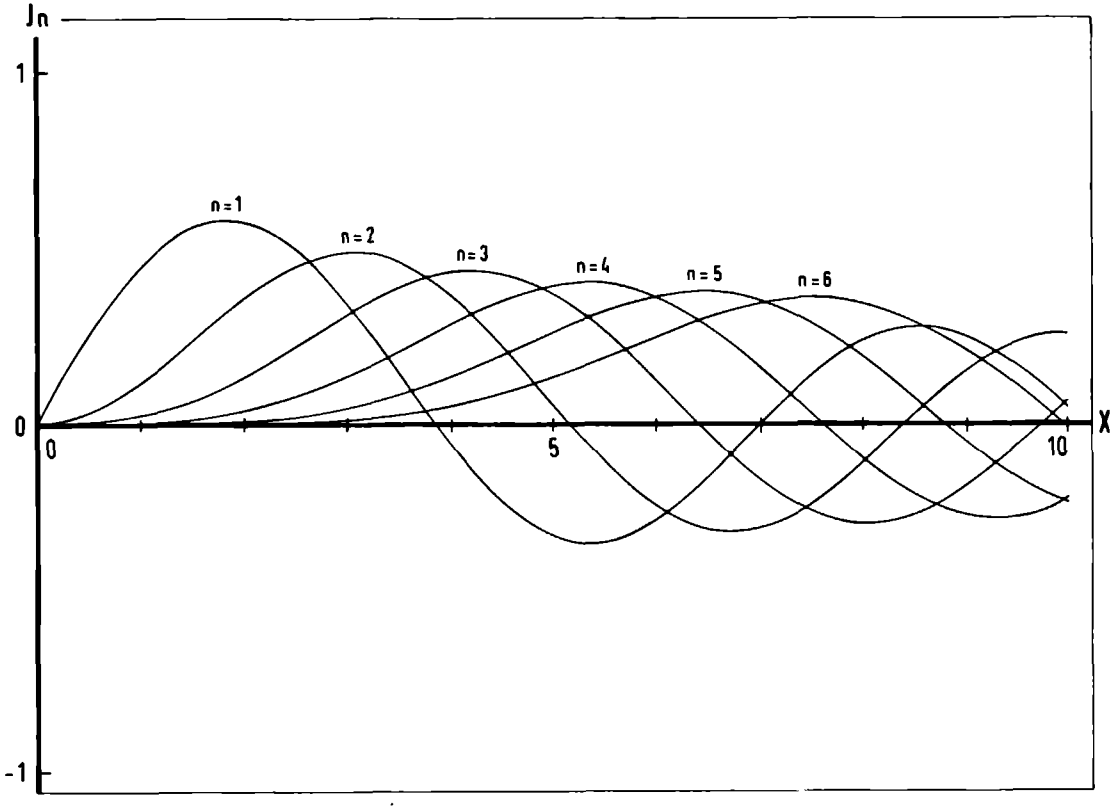

Fig. III-1 The Bessel functions of the first kind of order 1 till 6.

$$V = G \sum_{r=1}^{\infty} \sum_{n=1}^{\infty} 2n\omega \sin n\omega t \; J_n (2\pi r \, Fh/H^2)$$

$$M_r \sin (2\pi r(F/H - \gamma) + \theta_r + n\pi/2)$$

$$= \sum_{n=1}^{\infty} V_n \, n\omega \sin n\omega t$$

where r is the dHvA harmonic number, J_n is the Bessel function of the first kind of order n (fig. III-1) and G is the gain of the detection system. With a lock in it is possible to detect the amplitude of the signal with the desired frequency $n\omega$. In the present experiment the fourth harmonic (n=4) is chosen

$$V_4 = G \sum_{r=1}^{\infty} J_4(2\pi r Fh/H^2) \; M_r \sin(2\pi r(F/H-\gamma) + \theta_r).$$

To register the dHvA oscillations at a constant rate in time it is necessary to sweep the inverse of the magnetic field proportional to t. The sweep unit is described by N. Coenen (1976).

The dHvA waveshape is measured by taking a short block (10 fundamental oscillations) of digitized data at temperature T and mean field H in about five minutes. The modulation amplitude h is chosen in such a way that J_4 is at its first maximum for the third dHvA harmonic. In order to keep the argument of the Bessel function at the same value h has to be swept proportional to the square of the field H. The modulation frequency is 19 Hz.

The data is very carefully taken. Every sweep is done from low field to high field. Before sweeping the field is lowered and then set for the starting point to take care for hysterysis (Terwillinger, Higgins, 1972; Lengeler et al., 1977) and a short time is waited until "stability" is attained.

A diagram of the dHvA spectrometer is shown in fig. III-2. The compensation network consists of a condenser and a resistor which

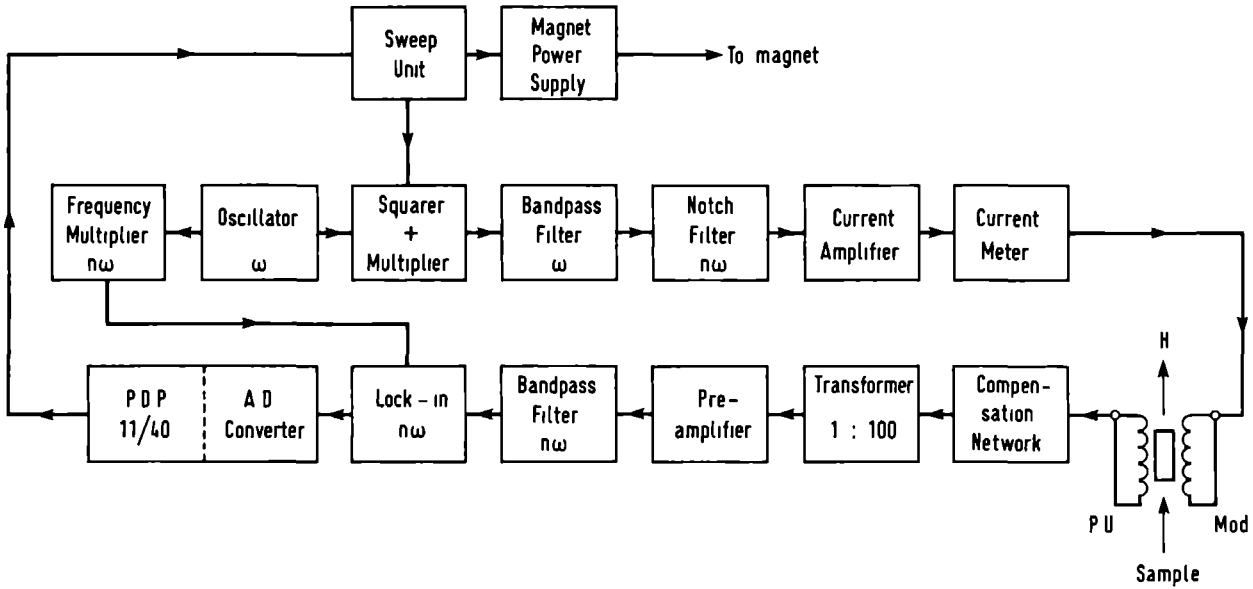

Fig. III-2 The electronic set-up.

can be switched parallel to one of the two pick-up coils, so that the voltages induced by the modulation field can be compensated better (about 100 dB).

The linearity of our analog-digital converter (12 bits) is ± .02%.

By sine-cosine fitting the data block (see appendix) it is possible to deduce the phases and the amplitudes of the dHvA harmonics. These amplitudes still contain the Bessel function and the gain G. For the observables M3122, M21 and M31 G drops out. The phases can contain a π depending on whether an accidental sign reversal has taken place.

Corrections for damping introduced by time-constants in the electronics or by digital manipulations have to be made.

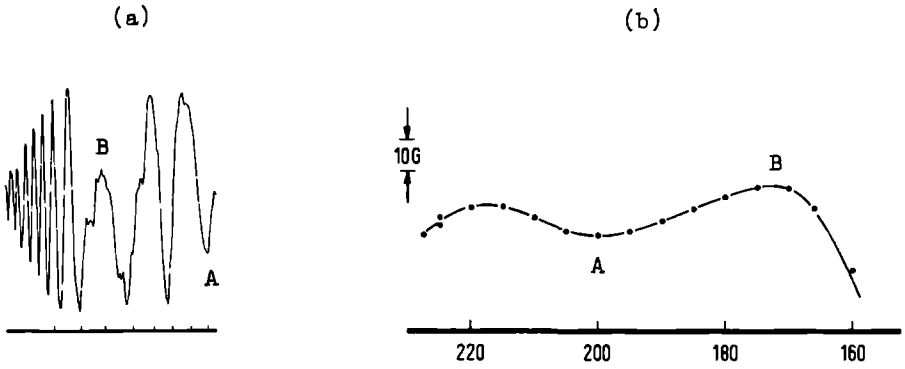

Fig. III-3 Lowering the sample holder causes a change in the phase of the dHvA signal ($F = 4.49\ 10^4$ T, $H = 4.42$ T). Every complete oscillation is a field shift of $P = H^2/F = 4.4$ G $= .44$ mT. The damping of the amplitude is caused by phase smearing through inhomogeneity of the magnetic field. The distance between two markers is 5 mm. A and B correspond to those in (b). The field profile of the magnet constructed from (a) at 7.07 T. The x axis is in millimetre. A and B correspond to those in (a).

Measurement is performed in a liquid ^{4}He bath containing a niobium titanium superconducting magnet of Oxford Instruments with a maximum field of 9 T at temperatures between 1.4 and 4.2 K achieved by lowering the gas pressure in the cryostat. The gas pressure is measured through the insert by a Wallace Tiernan meter.

The homogeneity of the magnetic field H over the crystal is very important because of the high phase factor 2π F/H of the dHvA effect. For the belly orbit in a noble metal (F ~ 5 10^4 T) at H = 5 T the phase factor change will be of order unity over the sample for $\Delta H/H = 10^{-5}$ (the damping factor for the amplitude is $\sin(\pi V)/(\pi V)$ for a right circular cylindrical crystal with its long axis parallel to H and also lying along a crystallographic direction for which $\partial F/\partial\theta = 0$ - i.e. a turning point of the dHvA frequency - with $V = \Delta HF/H^2$ (ΔH the change of magnetic field over the sample length), Hornfeldt et al., 1973; Paton and Slavin, 1973).

Thus the field profile of the magnet is measured by changing the position of the sample holder and looking at the phase shift of the dHvA signal (fig. III-3a) (Lowndes et al., 1973). Every oscillation is a change of the magnetic field which corresponds to one period P of the dHvA oscillation ($P = H^2/F$). Fig. III-3b gives the constructed field profile. The homogeneity over the sample is better than 10^{-5} in a region of 5 mm around the centre what gives a decrease of the amplitude smaller than 10% for the belly. Thus the sample has to be centred accurately.

Another problem is the drift of the magnetic field causing a change of the phase of the measured dHvA signal. This change can be measured by recording the phase of the dHvA signal in time when a constant sweep voltage is applied. The measured drift is small-

er or about .01% in 10 minutes what is too big for a good Fourier transform (phase shift for the belly ($F \approx 5\ 10^4$ T) at 5 T on a data block of about 30 periods is 360^o), but the drift during careful sweeping can be better than .001% (see section IV.1).

The magnetic field and its linearity is calibrated with an accuracy of .02% by counting the number of oscillations of e.g. the belly at <111> between two field values.

III.3 Modulation field

The modulation field is supported by a pair of Helmholtz coils with a calculated inhomogeneity over the sample of about 2%, with inside two pick-up coils (fig. III-4). For compensating the high voltage induced by the modulation field an identical pick-up and modulation coil pair is mounted nearby and connected antiparallel (Lowndes et al., 1973).

For waveshape analysis we must know the Bessel function factors of the first three harmonics or its ratios. By setting the current of the modulation field on the first Bessel zero of a dHvA signal a calibration of the modulation field can be done, but in practice this is not accurate enough (a deviation of 1% on the modulation field gives 4% in the amplitude of the fundamental). Measuring the amplitude of the first harmonic at 1, 2 and 3 times the modulation current of the to be analysed data-block gives directly the ratios (Alles and Higgins, 1974). Fitting the Bessel function on these three measured amplitudes even gives a better result, but then we rely heavily on the ideal performance of e.g. filter and transformer (Springford, 1971, reported a mixing of J_2 and J_0 for 2ω detection.)

The inhomogeneity of the modulation field affects the Bessel function. The function is replaced by an integral of the Bessel function over the sample volume (Springford, 1971).

An analogous problem is the inhomogeneity caused by the unequal penetration of the modulation field in the sample (skindepth problem), which also changes the detection phase of the lock-in if H is varied (Springford, 1971; Alles, Higgins, 1974; Knecht et al., 1977). To avoid skin-effect problems we have chosen 19 Hz as modulation frequency. Calculation of the skindepth δ with a resistance ratio of 30 for Au with 113 ppm Cr, gives δ = 1.5 mm. For pure gold the magnetoresistance guarantees a homogeneous penetra-

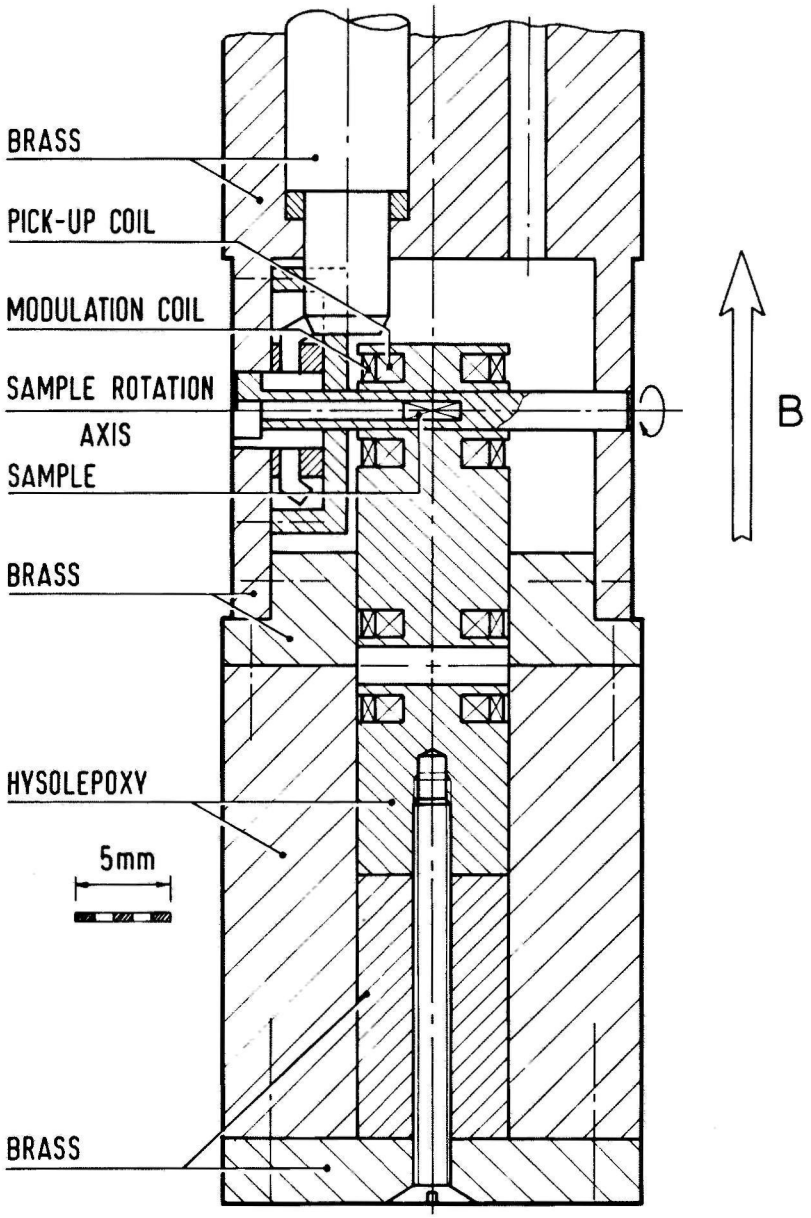

Fig. III-4 The sample holder used for measuring dHvA oscillations The sample can be rotated through 360°.

tion for all orbits except for the belly <100> and the dogbone <110> orbits. However, about half a degree away from these high symmetry directions the magnetoresistance is already large enough for the skindepth to be a problem (Lengeler, 1978). If the skin depth is smaller or of the same order of magnitude than the sample diameter then the Shubnikov-de Haas effect, an oscillatory resistance versus magnetic field with the same frequency as the dHvA gives rise to a pseudo-dHvA-signal (Terwillinger, Higgins, 1972; Knecht et al., 1977).

Sample heating due to the eddy-current effects can result in a difference between the sample temperature and the temperature of the liquid helium bath (for our samples this temperature difference is smaller than .005 K, Devillers, private communication). This can affect the amplitude of the signal and has to be proportional to square of the amplitude of the modulation field.

By measuring the amplitudes of the dHvA harmonics as a function of the modulation current at different magnetic field, for different orbits and temperatures, we could change the argument of the Bessel function $x = 2\pi rFh/H^2$ in a controllable way (fig. III-5). Non-linear least square fits (Brandt, 1970; Eadie et al., 1971) to J_4 allow the conclusion that we know the Bessel function factors of the first three harmonics with an accuracy of about .1%. Thus the above mentioned problems doesn't introduce mistakes on our fit on the three measured amplitudes (see second paragraph of this section). In fig. III-6 the two channels of the lock in (detection on 2ω) are compared.

We also used a superconducting modulation coil, which is composed of two coils separated .58 mm, with a total length of 52.58 mm and a bore of 13 mm (axial homogeneity over ±6 mm ± 1%), together with a sample holder containing only a compensated pick-up coil, with a spiral gear (Windmiller, Ketterson, 1968; Thorsen, Berlincourt, 1963).

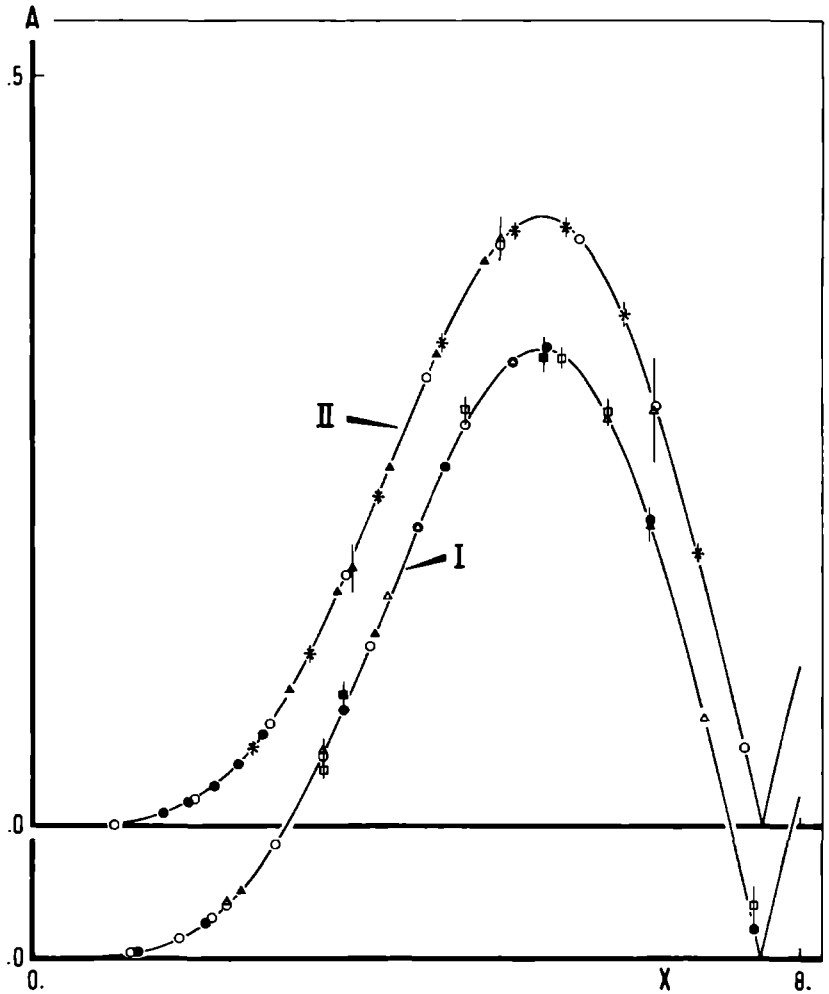

Fig. III-5 The amplitudes of belly oscillations (*) and of the first (o,●), second (Δ,▲) and third (□,■) harmonic of the neck at <111> versus the argument x of the Bessel function, which is fitted for the fundamental of the neck of one series (accuracy ≤ .1%) and then used for the other harmonics and orbits. In I H is 4.899 T (open figures) and 4.165 T (closed figures) at about 1.5 K. In II open figures at 4.356 T and 1.75 K, closed figures at 7.744 T and 4.22 K, and the asterisks at 8.823 T and 1.79 K.

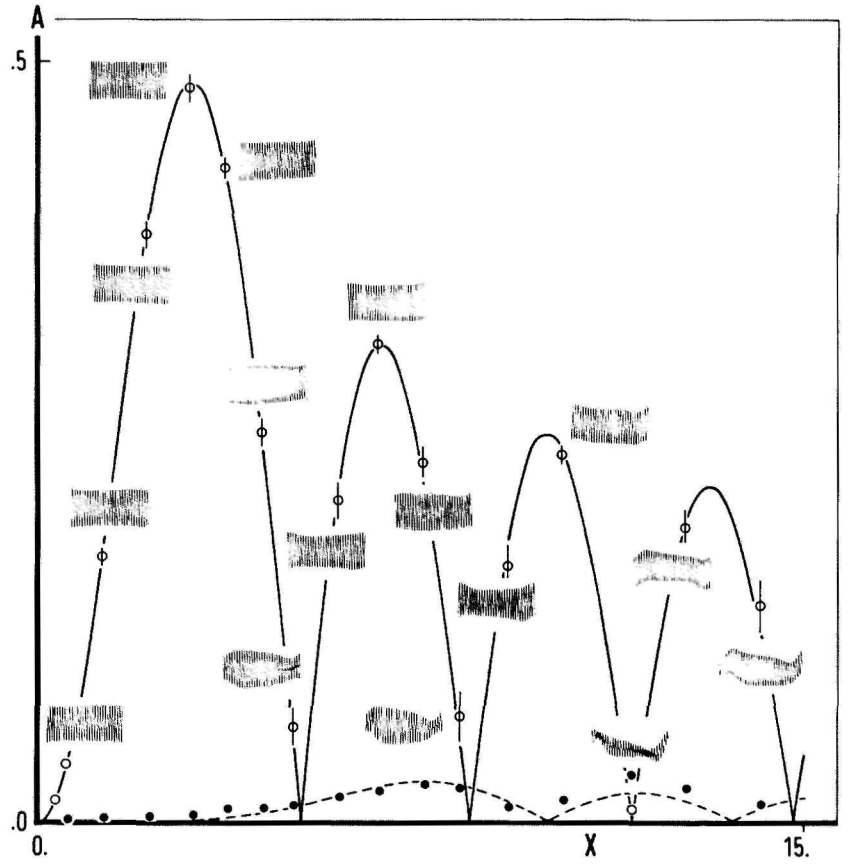

Fig. III-6 The in-phase amplitude (o) with the fitted $|J_2(x)|$ (solid line) and the quadrature amplitude (•) with the $|J_6(x)|$ (broken line) of the fundamental of the belly in the <111> direction, in the two channels of the lock-in amplifier (same units) versus modulation current (detection 2ω). The quadrature is a mixture of 2ω and 6ω signal (a consequence of the use of a lock-in). The small figures are the corresponding data blocks to the measured amplitude in the principal channel. The change of shape is caused by MI of the neck orbit.

III.4 Samples

A master alloy was grown of approximately 1 at. % Cr from 99.9999% Au and high-purity Cr and diluted to yield the desired impurity concentration during subsequent modified Bridgman growth with a steep temperature gradient for preventing crystal defects in pyrolytic Boron Nitride crucibles. After growth the crystals were oriented using Laue X-ray backscattering. The samples were cut from the large single crystals by spark cutting and carefully etched to size and finally annealed in high vacuum at ± 650°C for several hours. The shape of the samples is right parallelepiped (diameter 1.3 mm and length between 2.6 and 4.0 mm). The rotation axis is <110>. The specimens are fixed with some cotton-wool in the sample holder.

In order to check the crystallographic quality of the samples after mounting in the sample holder it was a general practice to rotate the sample around the principal axes at constant magnetic field. F is a function of the angle thus the phase of the sine (eq. II.1) varies which gives a signal like fig. III-7 (the phase of the belly at <111> and 8 T is about 5600 x 2π radians; changes of $\pi/2$ radians are easily detectable). These rotation diagrams have to be perfectly symmetric at the axes of the crystal and need a 180° symmetry. This latter is rather difficult to achieve because a mounting inaccuracy of .1° and a rotation shaft misalignment of .1° are not accurate enough. The magnetic field also has to be absolutely steady during rotation. A slightly strained sample or a sample with a structure of even very small misaligned crystals (which cannot be detected by Laue X-ray pictures) will show beat patterns on the field rotation diagram and on the field sweep diagram (a bad sample).

During rotation F changes, as well as the argument of the Bessel function. It can occur that the Bessel function goes

through zero producing an artificial beat pattern, which can be removed by changing the modulation current. A more serious problem is a beat pattern caused by a changing exchange field or g-factor as a function of orientation (eq. II-15). Only by comparing samples it is possible to distinguish between this and a sample with strain or mosaic structure.

Fig. III-7 (next page)
Rotation diagrams of orbits in selected samples (considered as good):
(a) dogbone,
(b) belly (fast one) and neck,
(c) neck with second harmonic,
(d) neck, belly and higher harmonics,
(e) turning point (A = 22^{o}; <100> to the left),
(f) belly beated by MI through the neck;
(a), (b) and (f) same sample.

Fig. III-8 (opposite of next page)
Rotation diagrams of orbits in samples with strain or mosaic structure:
(a) dogbone,
(b) belly,
(c) belly,
(d) belly,
(e) dogbone,
(f) neck;

(a) and (b) same sample;
(d), (e) and (f) same sample.

Fig. III-7

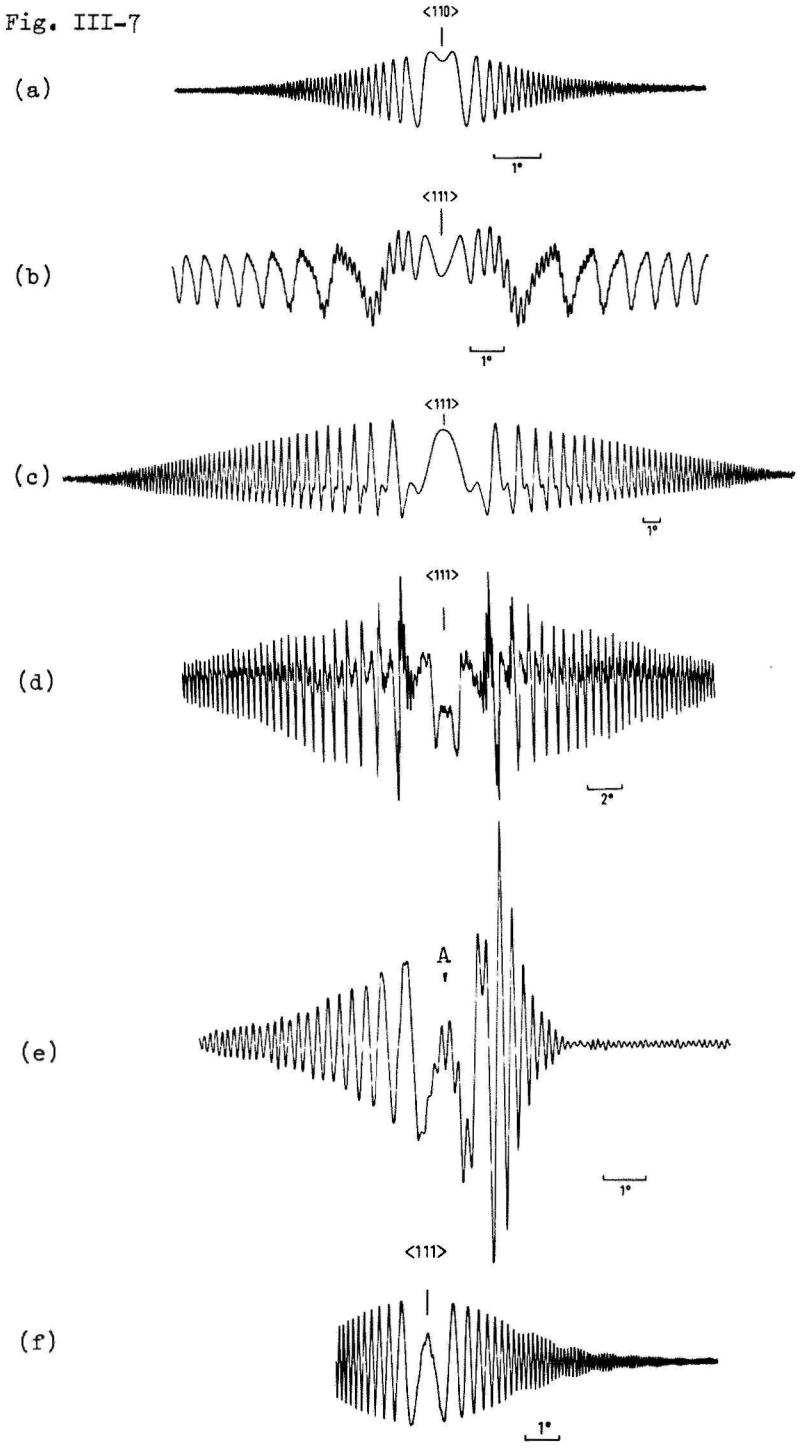

Fig. III-8

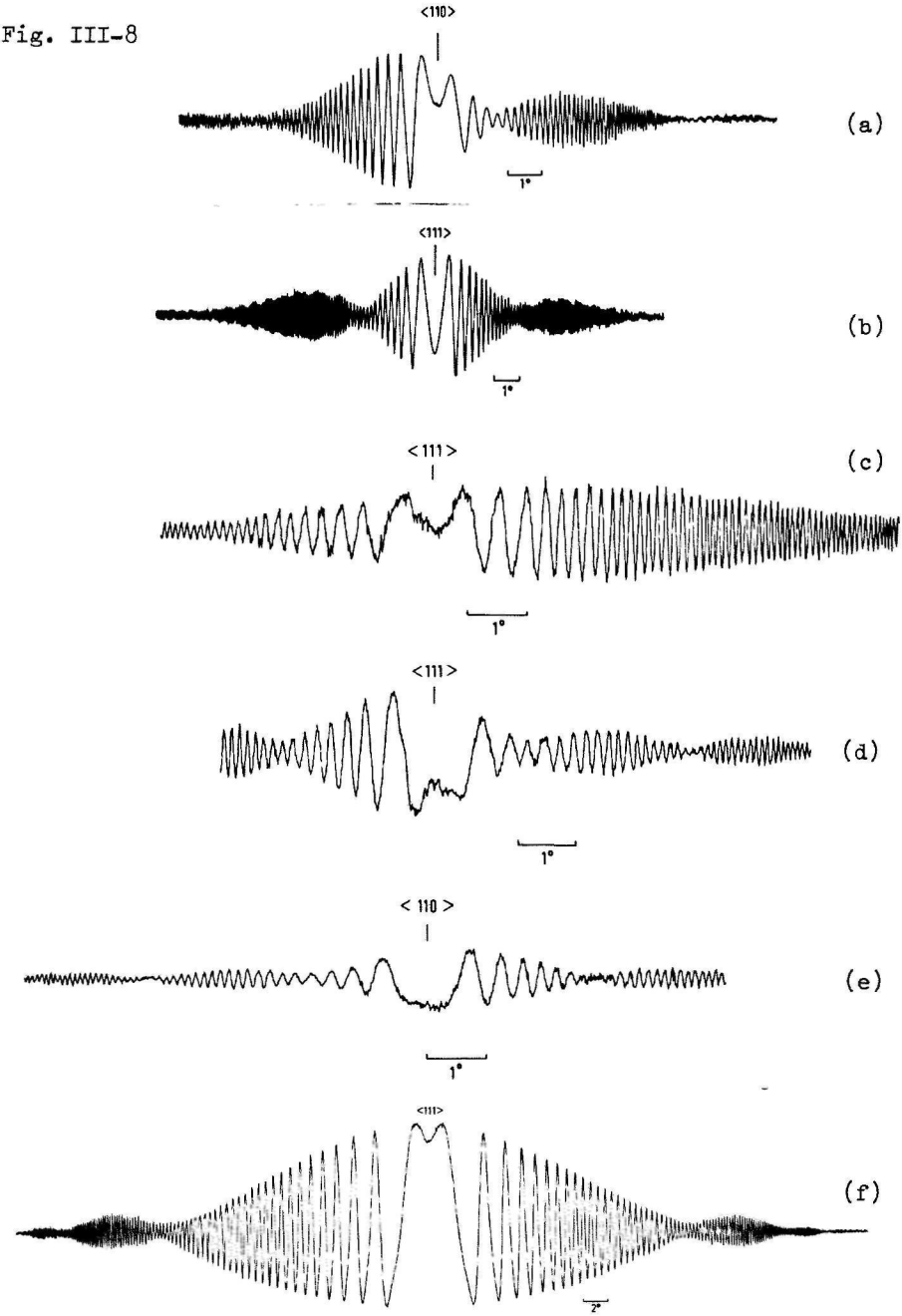

IV. Measurements and results

IV.1 Introduction

We have investigated six extremal orbits on the Fermi surface of gold-chromium alloys, for which $\partial F/\partial\theta=0$: the belly and the rosette with the magnetic field direction at <100> (B <100>, R <100>), the neck and the belly at <111> (N <111>, B <111>), the dogbone at <110> (D <110>) and the <100> "belly" orbit 18° from <100> toward <111> (TP18). For all these orbits the magnetic field is in the (110) plane. Off-symmetry orbits ($\partial F/\partial\theta\neq0$) are not investigated because mosaic spread could enhance the Dingle temperature and might vary appreciably from sample to sample (Miller et al., 1972). For a detailed knowledge of the Fermi surface of gold and its parameters see reference 3, 7, 31, 36 and 41

For every concentration (113, 230, 365 and 715 ppm) two or more good samples (section II.4) are selected.

Before analysis the data-block is rescaled, so that the signal of the data-block is a periodic function of 1/H.

For samples with ellipsoidal shape the demagnetization field is constant over the volume of the sample. Our samples are normally right parallelepipeds. The demagnetization field is inhomogeneous in these samples. Crabtree (1977) showed that it is possible to describe the dHvA signal with an average demagnetizing field for a cylindric and cubic sample. We have calculated the demagnetization factor N_e for our samples with fig. 2 of Crabtree (1977), assuming that our samples are degenerated cylinders. We have compared the microscopic parameters (H_{ex}, δX, X) from measurements on cubic and cylindric samples. Within experimental error there are no differences between these parameters.

Also blank measurements on pure gold and gold alloyed with .98 at. % silver (no magnetic impurities) give us $\delta X\sim.0$ and $S'\sim.16$

(table IV-1). These two examples demonstrate that the calculated N_e is correct for our samples.

As said before for a given concentration at least two 'good' samples were used. The microscopic parameters are identical within the experimental errors; only X, as is known, can differ from sample to sample because of strain etc.

For this reason we give the lower X value for each concentration.

	δX (K)	X (K)	S
Au (pure)	-.006 ± .006	.23 ± .03	.161 ± .003
Au[Ag]$_{.98}$ at. %	.04 ± .03	2.63 ± .06	.159 ± .002

Table IV-1 Results of the wave-shape analysis on the N <111> for pure gold and gold with .98 at. % silver. The S for pure gold is .157, .155 (Crabtree et al., 1975), .176 (Randles, 1972) or .146 (Alles et al., 1975). The finite Dingle temperature for pure gold demonstrates the existence of dislocations (Lengeler , 1977; see also fig. IV-4).

The N <111> is the only orbit which can be investigated by the wave-shape analysis technique in our samples, because the harmonic content of the other orbits is too strongly dominated by magnetic interaction (see section IV.2).

The eight observables (eq. II-38 to 45) are used for analysis. The following values for the neck parameters are used:

$1/\sqrt{\xi}$ = .26 (Bibby et al., 1979; Crabtree et al., 1975),

μ = .28 (Lengeler et al., 1977),

F = 1.5312 10^3 T (Coleridge, Templeton, 1972) and

S (pure gold) = .157 (Crabtree et al., 1975).

The electronic gain G of the set-up (section III.1) calculated with the observables (section II.3) is constant within 1% as temperature and magnetic field is changed. This has been checked with the lowest concentration. Of course G depends on the sample used.

For pure gold $S = (\mu/2)g_c$ (eq. II-4). As a function of the rotation angle θ it happens that $\cos(\pi S) = 0$ at a certain angle. The first harmonic of the dHvA signal then has a vanishing amplitude. On Au-Cr we have $S' = \mu/2(g_c+H_{ex}/H)$ (eq. II-15) and a minimum (no zero because $\delta X \neq 0$) amplitude shifts to a larger value of θ. These observations together with the experimental fact that S is an increasing function of θ (Crabtree et al., 1975), imply a negative value of H_{ex} (anti-ferromagnetic exchange, $J<0$, eq. II-9).

The multiplicity of solutions (section II.3) is resolved by the condition that H_{ex} and δX change in a physically reasonable manner as a function of H, T and c.

The final results can be found in fig. IV-1 to 3. From the small negative slope of X versus H (fig. IV-1) we conclude a decrease of spin-flip scattering of the conduction electrons if H is

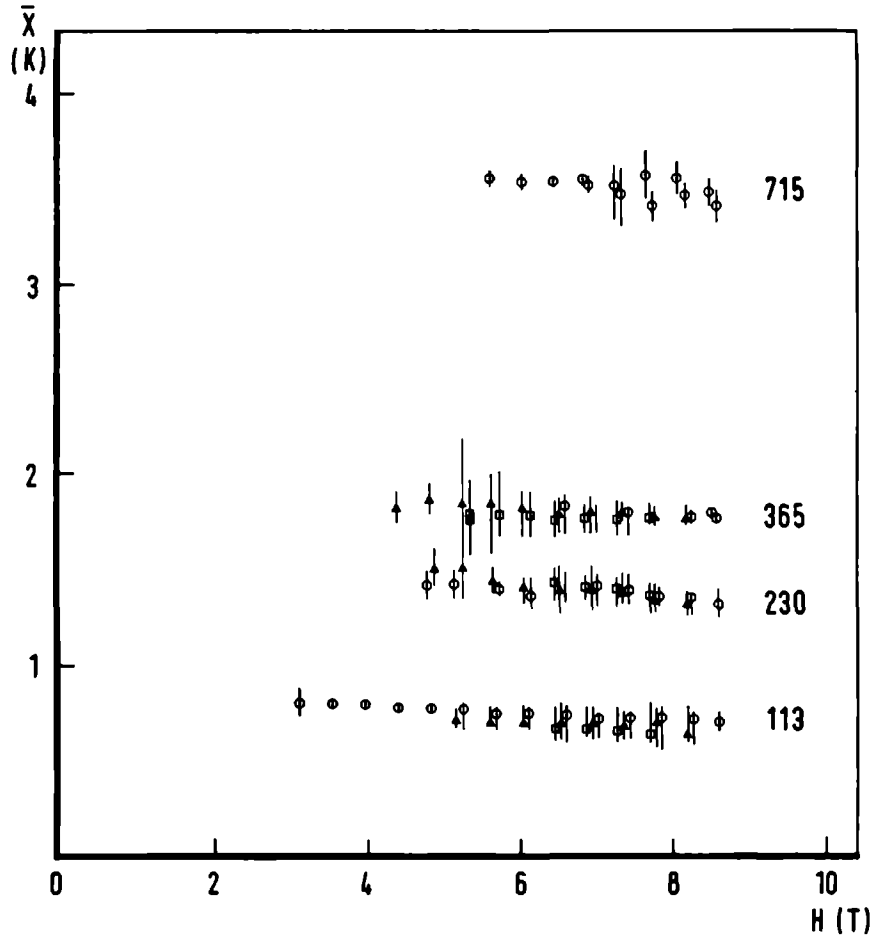

Fig. IV-1 The Dingle temperature X measured at 4.2 K (□), 3.0 K (▲) and ~1.6 K (o) versus H for four gold crystals with 715, 365, 230 and 113 ppm Cr. The points are shifted somewhat for clarity of the figure.

increased (due to increasing polarization of the local moment $\langle S_z \rangle$ of the impurity). X has no temperature dependence.

δX versus H (fig. IV-2) has a slightly, systematically positive slope. About temperature dependence no conclusion is possible.

δX and X demonstrate the different rates at which the freeze out of scattering occurs for spin up and spin down electrons (Lowndes, Reinders). This effect had been suggested by Béal-Monod and Weiner (1968) as the source of the "anomalous" negative magnetoresistance in dilute alloys containing d-shell local moments.

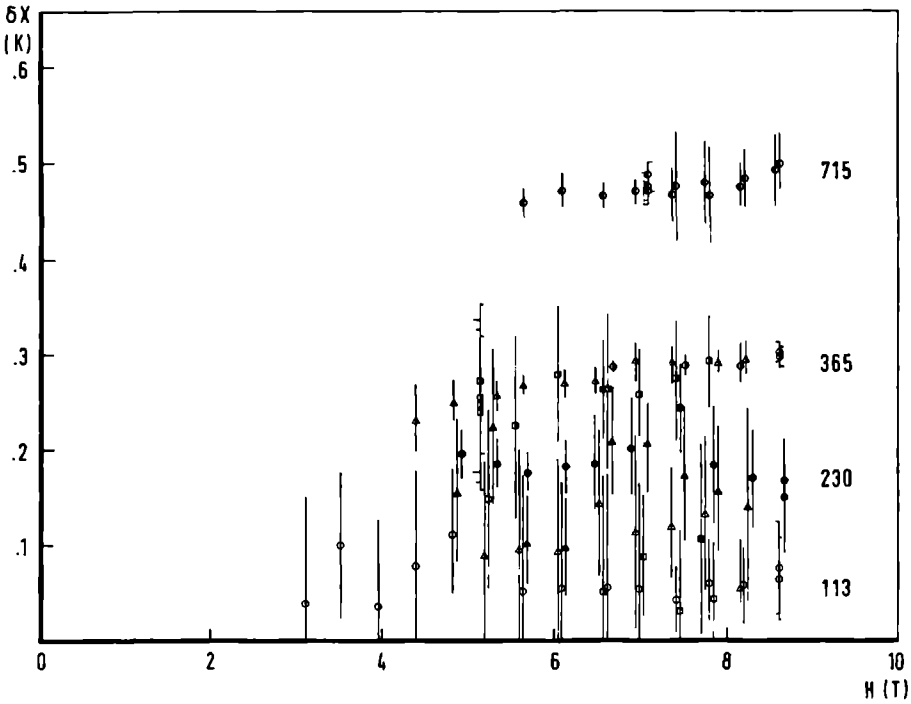

Fig. IV-2 For the same crystals as in fig. IV-1 δX versus H for 113 (open), 230 (closed), 365 (left side open) and 715 (right side open) ppm Cr in Au at temperatures of ~1.6 (o), 3.0 (Δ) and 4.2 K ($\square$). The points are shifted somewhat for clarity.

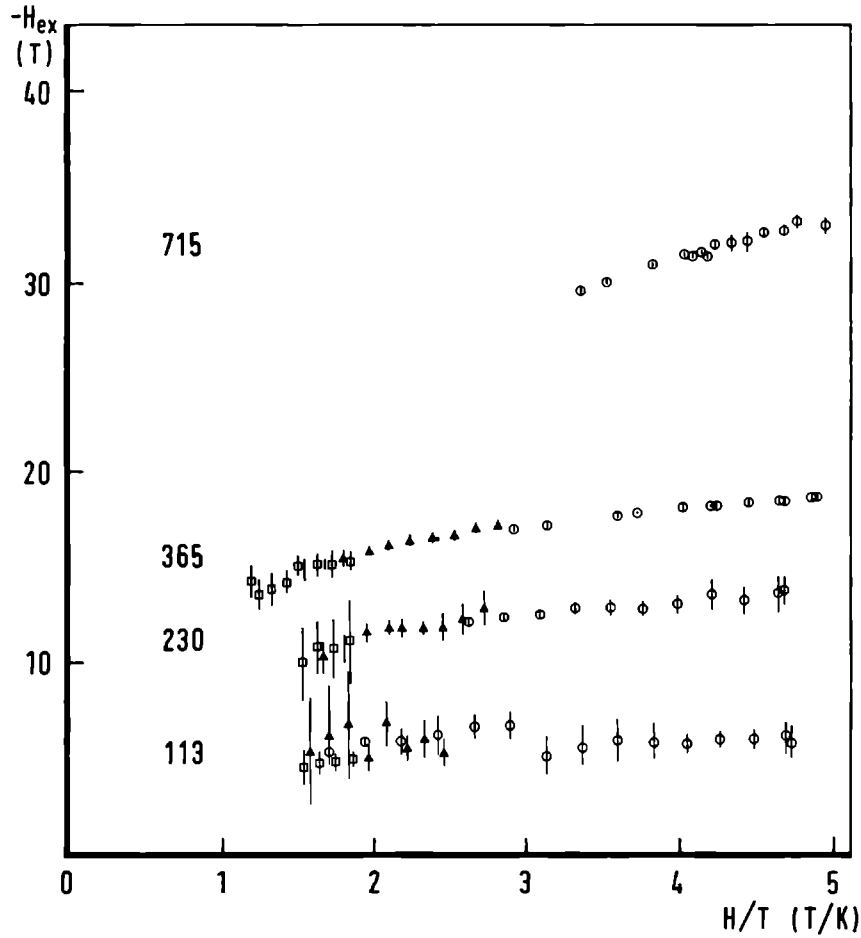

Fig. IV-3 The exchange field H_{ex} of the crystal as in fig. IV-1 (the same notation) versus H/T.

The exchange field is plotted versus H/T (fig. IV-3). This figure demonstrates the behaviour of H_{ex} as expected for an impurity moment near saturation in the applied magnetic field. From Fenton's theory a Langevin function results for the exchange field instead of a Brillouin function (Fenton, 1976).

With a least square method straight lines are fitted to the data of X versus H for each sample. The fitted lowest Dingle temperatures X at 6.5 T versus chromium concentration c (fig. IV-4) give a straight line with an intercept at .25 K on the c = 0 axis, which is also the measured X for the pure gold sample (see table IV-1). The gradient of the line is 44.3 ± .3 K / at. % Cr.

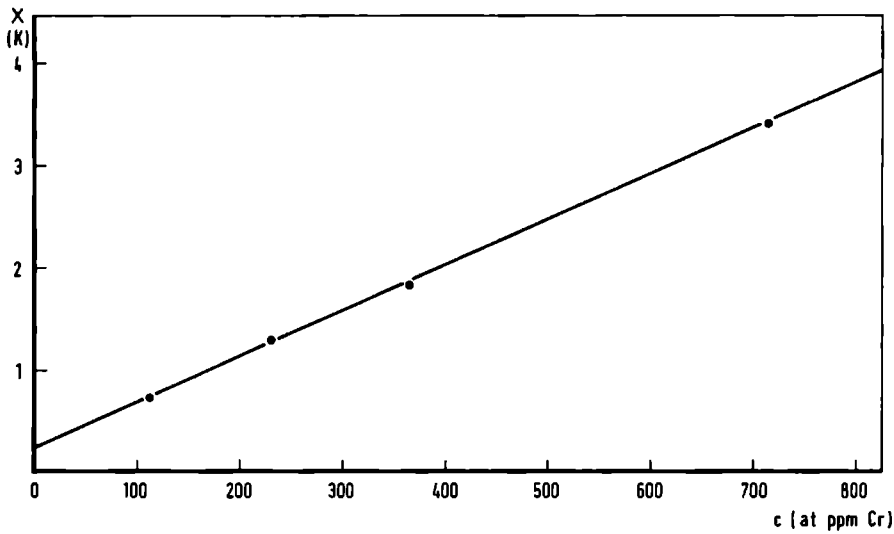

Fig. IV-4 The lowest Dingle temperature X at 6.5 T fitted on curves of fig. IV-1 for all samples from fig. IV-1 versus Cr concentration c. The errors are the size of the points.

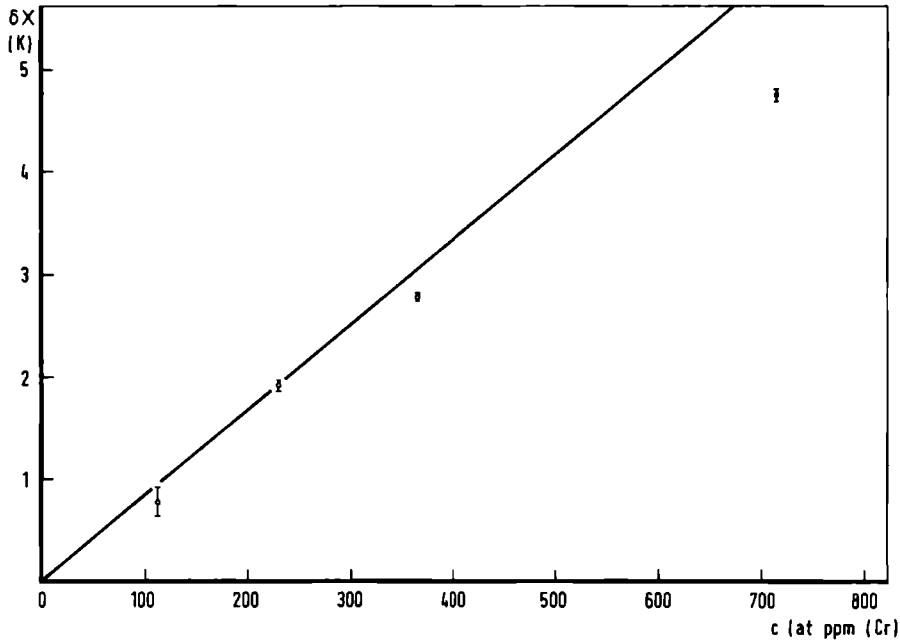

Fig. IV-5 The mean of fitted δX at 6.5 T on curves of fig. IV-1 versus Cr concentration with the corresponding error.

The same is done for δX (fig. IV-5). The values plotted are the means of the δX fitted at 6.5 T, of the samples with the same concentration. A parabola is fitted through the points together with the zero. The parameters are 8.66 ± .11 K/at.% and -28.9 ± 2.1 K/(at. %)^2.

H_{ex} versus H/T is fitted with a Langevin function and the mean values for H_{ex} at H/T = 4 T/K over the samples with the same concentration with the corresponding error bars, versus c is plotted in fig. IV-6. The parabola fitted through zero has as parameters: 576.6 ± 6.9 T/at. % and $-2.11 \pm .17$ kT/(at. %)^2.

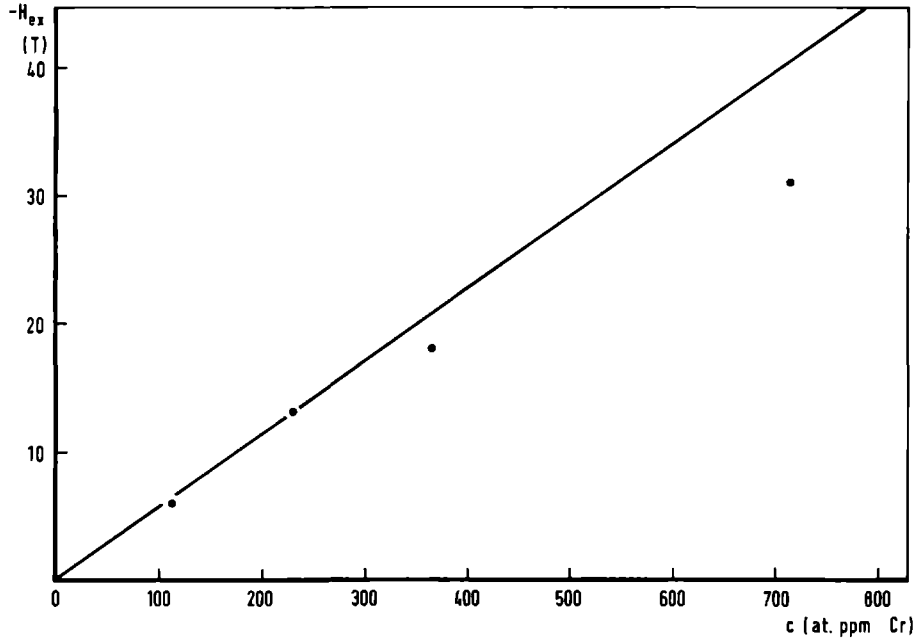

Fig. IV-6 The mean value of the exchange field H_{ex} at 4 T/K fitted on curves as shown in fig. IV-3 for all samples versus concentration with the corresponding error. The mean value per concentration is plotted. The errors are the size of the points.

The RKKY (Rudermann-Kittel-Kasuya-Yosida) interaction is a large range interaction (Bell and Caplin, 1975) which can couple magnetic impurities. H_{ex} and δX are pure magnetic properties and so these demonstrate a c^2 dependence.

On the contrary X is been made up of two components:
(1) one component caused by the valence and size difference between impurity and host,
(2) a magnetic scattering part caused by the spin of the impurity. The magnetic scattering is nearly freezed out. Only (1) is important thus X is directly proportional to c.

IV.3 The high frequency orbits

These larger orbits can not be investigated by the wave shape analysis technique because magnetic interaction (MI) dominates the amplitude and phases of the dHvA harmonics. However, by studying the amplitudes of the fundamental as a function of the magnetic field it is possible to deduce information on X, δX and H_{ex}, as we will show.

For this to be feasible it is necessary that first of all the usual Dingle plots

$$\ln\left|AH^{\frac{1}{2}}T^{-1}\ \sinh(\lambda\mu T/H)\right| \text{ versus } 1/H$$

show deviation from straight lines (fig. IV-7, 8).

Further the effect of MI has to be sufficiently small. This disturbing influence of MI can occur for the high frequency orbits in two ways.

a) Transfer of amplitude of the fundamental dHvA signal to and from the harmonics of the same dHvA orbit. For any Dingle temperature we have done an analysis leading to the conclusion that if T > 3 K this effect is negligible.

b) Intermodulation between B <111> and N <111> (Shoenberg, 1968) gives a repeating amplitude and frequency modulation over about 30 cycles of B <111>, as shown in fig. III-6 and also on the cover. To cope with this situation we take averages of the amplitude of 30 B <111> cycles. For the remaining high frequency orbits amplitude analysis takes place over 20 cycles of these orbits.

Detection is done on 2ω and 4ω with the field modulation amplitude chosen in such a way that the fundamental dHvA signal is on the first top of the respective Bessel function. Both detection frequencies give the same results.

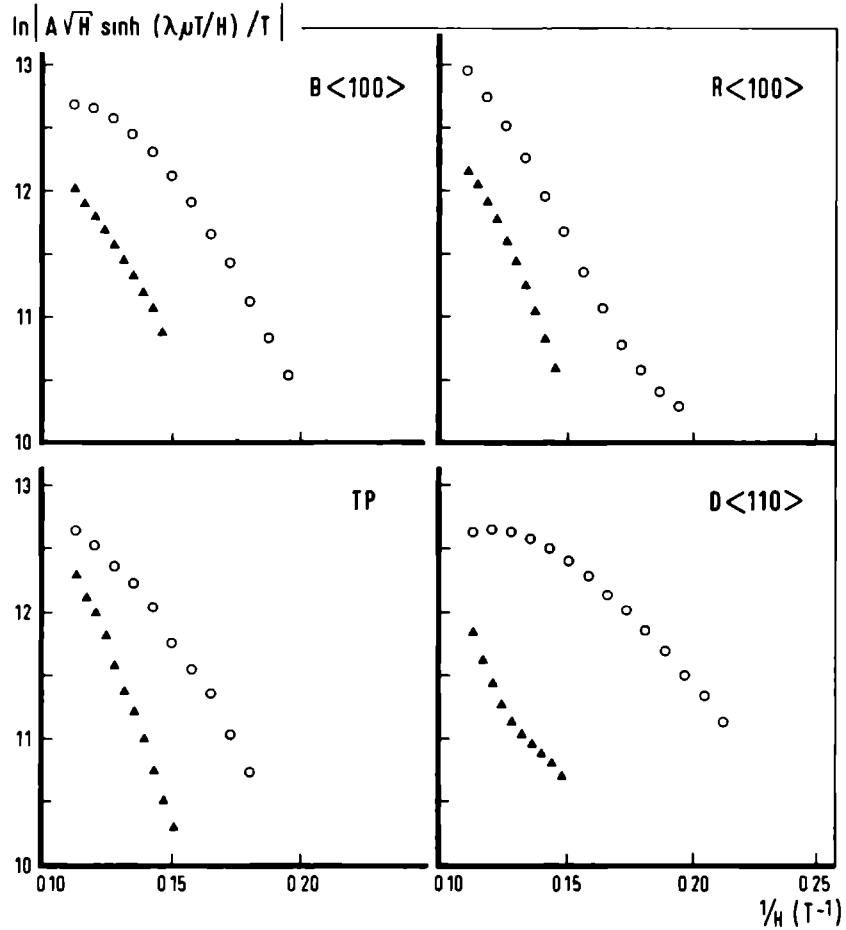

Fig. IV-7 Dingle plots for different cross sections in gold with 113 ppm (o) and 230 ppm (▲) chromium.

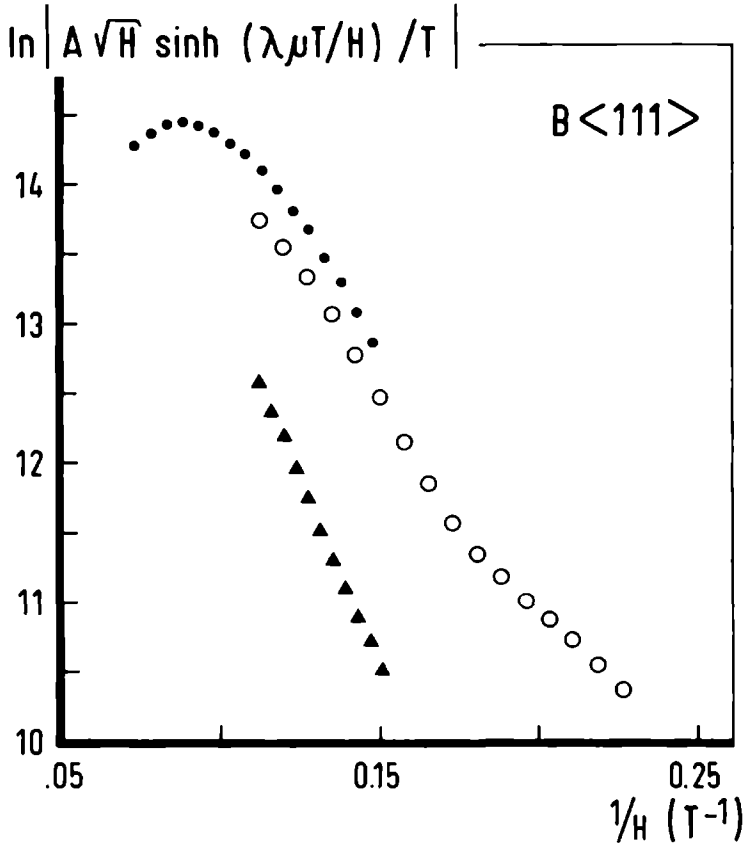

Fig. IV-8 Dingle plots for B <111> in gold with 113 ppm (o) and 230 ppm (▲) chromium. Also results in a 15 T Bitter magnet of Nijmegen Laboratory for High Magnetic Fields for another 113 ppm sample (●) are shown.

For non-magnetic impurities Dingle plots without magnetic interaction have to give straight lines with slopes proportional to the Dingle temperature (eq. II-3). The Dingle plots for the neck orbit of gold with chromium are nearly straight for "accidental" reasons.

Extraction of H_{ex}, δX and X from curved Dingle plots is only possible if we combine measurements on samples with two different concentrations; for this purpose 113 and 230 ppm were chosen. Further some simplifying assumptions have to be made. First of all we assume that the microscopic parameters (δX, X, H_{ex}) are independent on T and H. With the wave shape analysis data for the neck in fig. IV-1 to 3 in mind this seems to be a reasonable assumption. Secondly we assume also from the neck results that H_{ex} and δX are directly proportional to the Cr concentration whereas - the influence of strains in samples is not fully under control - the X's are allowed to be independent of the concentration c of the two samples. With these two assumptions we can fit the following formula on our data (fig. IV-7 and 8):

$$B \exp(-\lambda\mu X/H) \{\cosh(2\lambda\mu c\delta X/H) + \cos(2\pi(S + cH_{ex}/H))\}^{1/2}$$

(the amplitude of the first harmonic of eq. II-19) with the following parameters: B and X free for every sample, and both per atomic percent δX and H_{ex}, and S. Thus for the two samples we have to fit 7 parameters. The temperature factor was already divided out.

Normally two or more samples with nominal the same concentration were taken into account in the analysis. The X's are plotted versus concentration and a straight line is fitted in a "judicious" manner. The results are gathered in table IV-2 with the used effective masses μ. In table IV-3 S is compared with literature. The results show that it is possible to determine S with the same accuracy or even better with our technique than with other methods. Also the ambiguity in S caused by the cosine factor is resolved if the sign of the exchange field is known.

	μ	δX (K/at%)	X (K/at%)	$-H_{ex}$ (T/at%)
B <100>	1.142	14.7 ± 2.5	129.4 ± 4.4	1102. ± 28.
R <100>	1.014	18.6 ± 2.6	131.0 ± 7.1	1232. ± 115.
B <111>	1.066	23.27 ± .44	140.4 ± 5.8	1474. ± 12.
D <110>	.983	16.9 ± 1.7	123.0 ± 16.	1046. ± 18.
TP18	1.039	24.9 ± 2.4	176.0 ± 23.	1308. ± 77.
N <111>	.280	8.66 ± .11	44.3 ± .3	576.7± 6.9

Table IV-2 The final results of our fits on the Dingle plots of the high frequency orbits. The results on the N <111> are from the wave-shape analysis technique. The given μ, effective mass (Lengeler et al., 1977) is used in the fit.

	S Shoenberg et al. (a)			S Crabtree et al. (b)	S this work	g_c
B <100>	1.182	1.171	1.159	1.32	1.154 ± .039	2.021 ± .068
R <100>				.855 (1.15)	.80 ± .11	1.58 ± .29
B <111>	1.189	1.002	1.178	1.25	1.113 ± .011	2.088 ± .021
D <110>	.998	1.091 (.909)	.998	.856	1.005 ± .013	2.045 ± .026
TP18	1.086	1.143	1.1065	1.23 (.768)	1.120 ± .062	2.16 ± .12

Table IV-3 (a) These three columns give results of the absolute amplitude measurements of Bibby and Shoenberg (1979) for different geometrical models of the Fermi surface;
(b) gives the experimental results of Crabtree et al. (1977), between brackets the alternate solutions resulting from ambiguity in inverting $\cos(\pi S)$;
(c) the last column contains our results.

Appendix (sine-cosine fit)

A data-block (fig. A-1) consists of 4096 points. A linear least square fit of the amplitudes of a sine and cosine and its two higher harmonics (a Fourier transform by matrix inversion for given frequency) is done as a function of frequency. The fit with the lowest Q^2-value, the sum of residual squares, gives us the right frequency. Then the fit is done on the first N points of the data-block, N chosen in such a way that it contains two fundamental periods of the signal calculated with the right frequency. This window of N points is shifted hundred times over the data-block by equal amounts till the complete 4096 points are done. So we have for the amplitudes, amplitude ratio's, phases, or phase-differences and Q^2 arrays of 100 points for one data-block (see fig. A-2). The amplitudes have the desired shape: a decay caused by the Dingle and the temperature factor (eq. II-2,3). The fluctuations with respect to a straight line are caused by drifts in the frequency, unstable temperature, noise and higher order background. From the nature of irregularities in curves of fig. A-2 and A-3 the source of the irregularities can sometimes be found, providing means to remedy it. It is also possible to select out bad data-blocks and bad fits (e.g. a wrong frequency fit caused by a local minimum in Q^2 gives a slope in the phase F1).

By fitting a straight line on the hundred points of an amplitude or a phase we get the mean value and also the errors via the covariance matrix. In favourable cases we find that the errors for the amplitudes are ≈ .1%, and for the phases ≈ .3 degree.

This fitting procedure is introduced because a Fourier transform (F.T.) on the <u>complete</u> block is too strongly affected by drift (if the phase is changing in the data-block, the F.T. gives a lower value for the amplitude; the phase can also shift by the cosine factor (eq. II-20)) and background.

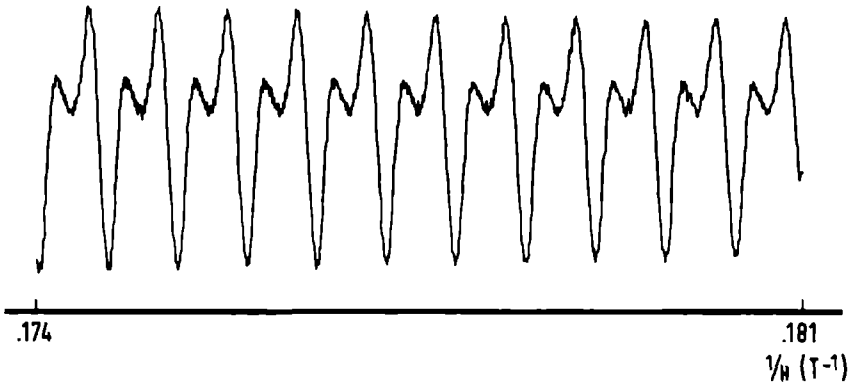

Fig. A-1 A typical data-block of the neck orbit.

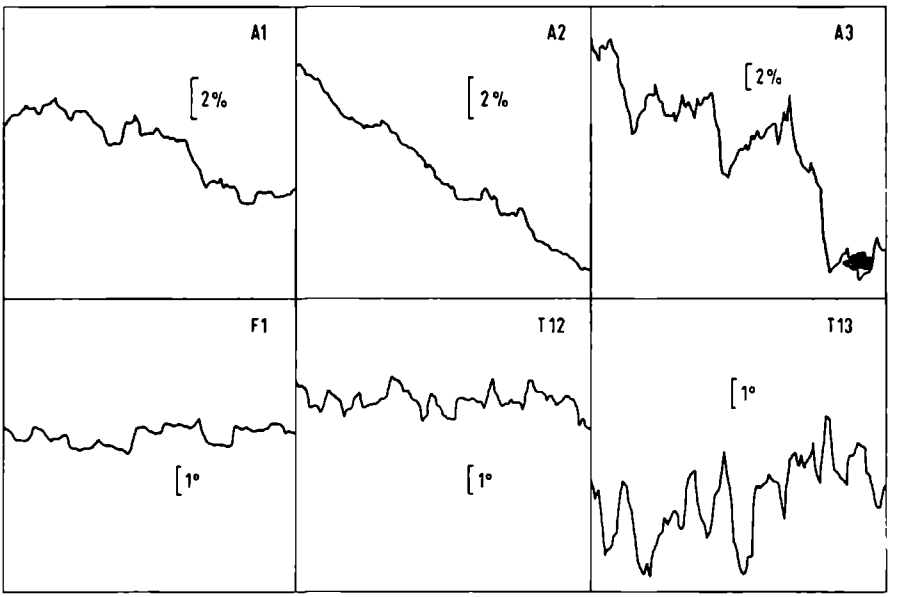

Fig. A-2 The arrays of the fit (see text) for the data-block of fig. A-1. A1, A2 and A3 the amplitude of the first three harmonics. F1 the phase of the first harmonic with respect to the beginning of the data-block. T12 and T13 the observables of eq. II-38 and 39. The bars correspond to the given change in the quantities.

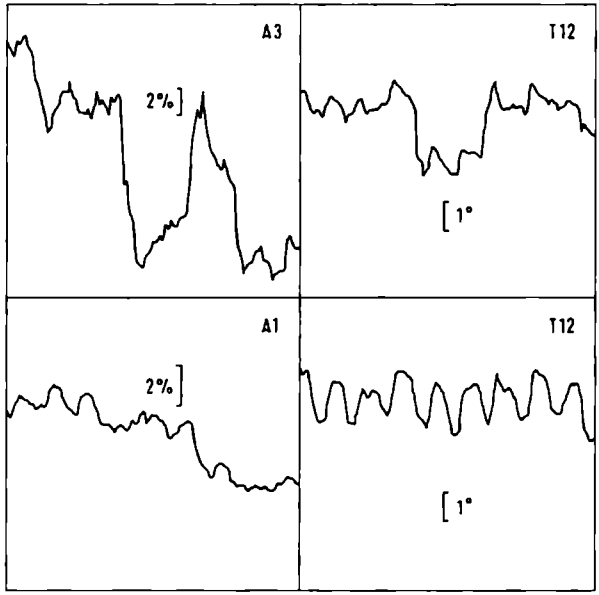

Fig. A-3 The same as in fig. A-2, however the above pictures show the result with an artificial spike in the data-block, and the two other pictures the result after second order background substraction. The pictures can be compared with the corresponding pictures in fig. A-2.

References

1 Alles H, Higgins RJ, Lowndes DH,
Phys. Rev. B 12 4, 1975, 1304-1313

2 Alles H, Lowndes DH
Phys. Rev. B 8 12, 1973, p. 5462-5472

3 Ashcroft NW, Merman ND
Solid State Phys.
Holt, Rinehart and Winston, 1975

4 Béal-Monod MT, Weiner RA
Phys. Rev. 190, 1968, p. 552-557

5 Bell AE, Caplin AD
Contemp. Phys. 16 4, 1975, p. 375-394

6 Bibby WM, Coleridge PT, Cooper NS, Nex CMM, Shoenberg D
J. of Low Temp. Phys. 34, 1979, p. 681-694

7 Bibby WM, Shoenberg D
J. of Low Temp. Phys. 34, 1979, p. 659-680

8 Blackman M
Proc. Roy. Soc. A166, 1938, p. 1-15

9 Bosacchi B, Ketterson JB, Windmiller LR
Phys. Rev. B 4 4, 1971, p.1197-1210

10 Brailsford AD
Phys. Rev. 149, 1966, p. 456-463

11 Brandt S
North-Holland Publishing Company, Amsterdam, 1970
Statistcal and computational methods in data analysis

12 Chambers RG
Can. J. Phys. 34, 1956, 1395

13 Chung Y, Lowndes DH, Hendel DL
J. of Low Temp. Phys. 32, 1978, p. 599-641

14 Coenen NJM
Proefschrift, K.U.N. (1976)
Het de Haas - van Alphen effect en het fermi oppervlak van PbSb

15 Coleridge PT, Scott GB, Templeton IM
Can. J. Phys. 50, 1974, p. 1999-2011

16 Coleridge PT, Templeton IM
J. Phys. F: Metal Physics 2, 1972, p. 643-56

17 Condon JH
Phys. Rev. 145, 1966, p. 526-535

18 Crabtree GW
Phys. Rev. B16, 1977, p. 1117-1125

19 Crabtree GW, Windmiller LR, Ketterson JB
J. of the Low Temp. Phys. 20, 1975, p. 655-675

20 Crabtree GW, Windmiller LR, Ketterson JB
J. of Low Temp. Phys. 26, 1977, p. 735-62

21 Dingle RB
Proc. R. Soc. A211, 1952, p. 500-516

22 Dingle RB
Proc. R. Soc. A211, 1952, p. 517-525

23 Eadie WT, Dryard P, James FE, Roos M, Sadoulet B
North Holland Publishing Co., Amsterdam 1971
Statistical methods in experimental physics

24 Engelsberg S, Simpson G
Phys. Rev. B2 6, 1970, p. 1657-1665

25 Fenton EW
J. Phys. F: Metal Phys. 6 3, 1976, 363-380

26 Fowler M, Prange PE
Physics 1, 1965, p. 315-328

27 Gold AV
Solid State Physics, vol.1: Electrons in metals, p. 39-126

28 Goldstein A, Williamson SJ, Foner S.
Rev. Sci. Instrum. 36 8, 1965, 1356-1365

29 de Haas WJ, van Alphen PM
Leiden Comm. 208 d, 1930, p. 31-33
Reprinted from Proc. Kon. Akad. Amsterdam: 33, 1930, p. 680;

30 de Haas WJ, van Alphen PM
Leiden Comm. 212 a, 1930
Reprinted from Proc. Kon. Acad. Amsterdam: 33, 1930, p. 1106

31 Halse MR
Phil. Trans. Roy. Soc. Lond. A 265, 1969, 507

32 Heeger AJ
Sol. State Phys. 23, 1969, p. 283 (editors F. Seitz, e.a.)

33 Higgins RJ, Lowndes DH
Waveshape analysis in the de Haas-van Alphen effect
in "Electrons at the Fermi surface", p. 393 reference 65

34 Hoch PK
Contemp. Physics 24 1, 1983, p. 3-23

35 Hornfeldt S, Ketterson JB, Windmiller LR
J. Phys. E 6, 1973, p. 265-268

36 Joseph AS, Thorsen AC, Blum FA
Phys. Rev. 140 6A, 1965, p. 2046

37 Knecht B, Lonzarich GG, Perz JM, Shoenberg D
J. of Low Temp. Phys. 29 5-6, 1977, p. 499-531

38 Kondo J
Progr. Theor. Phys. 32 1, 1964, p. 37

39 Landau LD
Z. Phys. 64, 1930, p. 629
also in Collected Papers of L.D. Landau by Ter Haar p. 31-38

40 Lengeler B
Phys.Rev. B 15, 1977, p.5504-5511

41 Lengeler B
Springer Tracts in Mod. Phys. 82, p. 1-67, Springer Verlag 1978
Electronic structure of noble metals

42 Lengeler B, Wampler WR, Bourassa RR, Wingeruth K, Uelhoff W
Phys. Rev. B15 12, 1977, p. 5493

43 Lifshitz IM and Kosevich AM
Zh. eksp. theor. Fiz. 29, 1955, p. 730
(English translation: Sov. Phys. JETP 2, 1956, p. 636-645)

44 Lifshitz IM and Kaganov MI
Sov. Phys. Uspekki 5, 1963, p. 878-907

45 Lowndes DH
J. Appl. Phys. 50 3, 1979, p. 2080-2085

46 Lowndes, Reinders
unpublished, see reference 33 and 45

47 Lowndes DH, Miller KM, Poulsen RG, Springford M
Proc. R. Soc. Lond. A331, 1973, p. 497-523

48 Miller KM, Poulsen RG, Springford M
J. Low Temp. Phys. 6, 5/6, 1972, p. 411-423

49 Onsager L
Phil. Mag. 43, 1952, p. 1006-1008

50 Paton BE, Slavin AJ
Rev. Sci. Instrum. 44 9, 1973, p. 1357

51 Peierls R
Z. f. Phys. 81, 1933, p. 186-194

52 Perz JM, Shoenberg D
J. of Low Temp. Phys. 25 3/4, 1976, p. 275-297

53 Phillips RA and Gold AV
Phys. Rev. 178, 1969, p. 932-948

54 Pippard AB
Proc. R. Soc. Lond. 272, 1963, p. 192-206

55 Randles DL
Proc. R. Soc. Lond. A 331, 1972, 85-101

56 Shiba H
Progress of Theor. Phys. 50, 1973, p. 1797-1823

57 Shoenberg D
Proc. Roy. Soc. 170A, 1939, p. 341-364

58 Shoenberg D
Nature 170, 1952, p. 569

59 Shoenberg D
Phil. Trans. R. Soc. A 255, 1962, p. 85-133

60 Shoenberg D
Can. J. Phys. 46, 1968, p. 1915-1923

61 Shoenberg D, Stiles PJ
Phys. L. 4, 1963, p. 274-275

62 Shoenberg D, Stiles PJ
Proc. R. Soc. 281A, 1964, p. 62-91

63 Shoenberg D, Vuillemin JJ
Proc. Tenth Int. Conf. Low Temp. Phys. Moscow 3, 1966,
p. 67, edited by MP Malkov

64 Springford M
Advances in Phys. 20 86, 1971, p. 493-550

65 Springford M
Cambridge University Press, Cambridge, 1980
Electrons at the Fermi surface

66 Stark RW, Windmiller LR
Cryog. october 1968, p. 272-281

67 Terwilliger DW, Higgins RJ
J. Appl. Phys. 43 8, 1972, p. 3346-3357

68 Thorsen AC, Berlincourt TG
Rev. Sci. Instrum. 34, 1963, p. 435-436

69 Windmiller, Ketterson
Rev. Sci. Instrum. 39, 1968, p. 1672-1682

70 Ziman JM Principles of the theory of solids
Cambridge University Press 1964

The first chapter of the thesis gives an historical description of the de Haas-van Alphen effect, an oscillatory behaviour of the diamagnetic susceptibility.

The second chapter gives an introduction in the theory of the dHvA effect with magnetic interaction and magnetic impurities. The wave-shape analysis technique is presented. The number of observable quantities which can be used in the analysis, is increased from 5, as was usual before, to 8. A computer-graphic technique provides precise values with error estimates for the exchange field and the scattering rates of the spin up and down conduction electrons.

An experimental technique, the large field amplitude modulation technique, is discussed in chapter three. Nearly all properties of the system are checked with the dHvA signal, for instance the homogeneity of the superconducting magnet. Special attention has been paid to the amplitude ratio's of the dHvA signal. These could be measured with an accuracy of about .1%. Skin effect, sample heating and inhomogeneity of the modulation field are discussed. Good samples are selected by interpretation of rotation diagrams.

The measurements and results are reported in chapter four. The neck orbit could be investigated by the wave-shape analysis technique in the samples (Au with 113, 230, 365 and 715 ppm Cr) between 1.5 K and 4.2 K at magnetic field values ranging from 3.5 to 9.0 T. We found a mean scattering rate of the spin up and down electrons of the neck orbit which is proportional with the chromium concentration. The exchange field and the difference of the scattering rates of spin up and down electrons are affected by impurity-impurity interaction caused by the Rudermann-Kittel-Kasuya-Yosida interaction. The scattering rates show a negative "magneto resistivity".

In the fourth chapter also a new method for analysing the high frequency orbits is described in the case that the Dingle plots are curved. By fitting the dHvA signal in two or more samples with different concentrations it was possible to get exchange fields, mean Dingle temperatures and differences in the Dingle temperature of the spin up and down electrons plus the S (g-factor) of pure gold. These g-factors have been obtained more accurately than by the normally used absolute amplitude measurements.

In the appendix a way of fitting sine and cosine waves is given. In contrast to Fourier transform techniques this fitting procedure is less affected by drifts in the dHvA frequency and has the advantage that assignment of errors in the observables can be estimated easier.

In het eerste hoofdstuk van het proefschrift wordt ingegaan op de historische ontwikkeling van het de Haas-van Alphen effect, een oscillatief gedrag van de diamagnetische susceptibiliteit.

Het tweede hoofdstuk geeft een introductie in de theorie van het de Haas-van Alphen effect met magnetische interactie en magnetische verontreinigingen. De "wave-shape analysis" techniek wordt besproken. Het aantal te meten grootheden, die gebruikt kunnen worden, is uitgebreid van 5 naar 8. Een computer gestuurde grafische techniek geeft preciese waarden met hun fout voor het "exchange"-veld en de mate van verstrooiing van de geleidingselectronen met spinimpulsmoment omhoog en omlaag.

Een experimentele techniek, de "large field amplitude modulation" techniek, wordt in hoofdstuk drie besproken. Bijna alle karakteristieken van de opstelling zijn m.b.v. het dHvA signaal gecontroleerd, b.v. de homogeniteit van de supergeleidende spoel. Speciale aandacht is besteed aan de amplitude-verhoudingen van het dHvA signaal. Deze zijn met een nauwkeurigheid van ongeveer .1% gemeten. Het indringdiepte-effect, de opwarming van het preparaat ten gevolge van het mudulatieveld en de inhomogeniteit van het modulatieveld worden besproken. Met behulp van rotatiediagrammen zijn goede preparaten geselecteerd.

De metingen en resultaten worden in hoofdstuk vier gepresenteerd. De "neck"-baan is onderzocht m.b.v. de "wave-shape analysis" techniek in goud preparaten met 113, 230, 365 en 715 ppm Cr bij temperaturen tussen 1.5 en 4.2 K en magneetvelden van 3.5 tot 9.0 T. We vonden een gemiddelde verstrooiingsmaat voor de electronen met spinimpulsmoment omhoog en omlaag voor de nekbaan, die rechtevenredig is met de chroomconcentratie. Het "exchange"-veld en het verschil van de mate van verstrooiing voor de electronen met spinimpulsmoment omhoog en omlaag worden door de

Rudermann-Kittel-Kasuya-Yosida wisselwerking tussen de verontreinigingen beinvloed. De mate van verstrooiing duidt op een negatieve magneto-weerstand.

In het vierde hoofdstuk wordt ook een beschrijving gegeven van een nieuwe methode om de hoogfrequente banen te analyseren indien de Dingle figuren gekromd zijn. Door het dHvA signaal van twee of meer preparaten met verschillende concentraties te fitten was het mogelijk "exchange"-velden, gemiddelde Dingle temperaturen en verschillen in de Dingle temperatuur van de electronen met de spin omhoog en omlaag plus de S (g-factor) van zuiver goud te bepalen. Deze g-factoren konden nauwkeuriger bepaald worden, dan m.b.v. absolute amplitude-metingen.

In de appendix wordt een andere manier om sinussen en cosinussen te fitten beschreven dan de normale Fourier transformatie. Deze fit procedure wordt minder beinvloed door het weglopen van de frequencie en heeft het voordeel dat de fouten eenvoudiger te verkrijgen zijn.

Curriculum vitae

P.H.P. Reinders

Middelbaar onderwijs:	1965 - 1968, Willibrordus-school (Mulo-A), Panningen 1968 - 1971, Blariacumcollege (H.B.S.-B), Venlo-Blerick
Universitaire studie:	1971 - 1977, natuurkunde, Katholieke Universiteit Nijmegen 1975: kandidaatsexamen 1977: doctoraalexamen (experimentele natuurkunde)
Promotieonderzoek:	1977 - 1982, afdeling Experimentele Natuurkunde I, Katholieke Universiteit Nijmegen.

Stellingen

I De bewering van T.L. Chow dat de canonieke bewegingsvergelijkingen verkeerd afgeleid zijn uit het Hamilton principe in Goldstein's boek, Classical Mechanics, is niet correct.

T.L. Chow, Eur. J. Phys. 1 (1980) 55-56

II De He^4 dampdrukschaal, die uitsluitend bedoeld is om gebruikt te worden voor kwikmanometers bij 20^o C op het Fysisch Laboratorium te Nijmegen, is verkeerd berekend en bovendien verouderd.

III Het is uit den boze dat sommige fabricanten specificaties van de door hen geleverde apparatuur slechts afleiden uit met de computer berekende tabellen i.p.v. uit gemeten grootheden.

IV Om verwarring te voorkomen zou het begrip Kondo-legering uitsluitend gebruikt moeten worden voor legeringen die een minimum in de weerstand vertonen als functie van de temperatuur en waarin de gast-atomen geen wederzijdse wisselwerking hebben (zowel direct als indirect).

V Het dynamische gedrag van apparatuur moet beter tot uitdrukking komen in bijgeleverde specificaties.

VI Het is aanbevelenswaardig om bij de kleinste kwadraten methode uitsluitend te spreken over Q^2 voor de som van de kwadraten van het gewogen residu i.p.v. χ^2, daar er al een χ^2 test bestaat.

VII De berekeningen van Terwilliger en Higgins met betrekking tot de invloed van het Shubnikov - de Haas effect op de de geinduceerd electrische spanning in het oppikspoeltje van een de Haas - van Alphen spectrometer zijn foutief.

D.W. Terwilliger, R.J. Higgins, J. Appl. Phys., vol.43 (1972) 3346-3357